International Journal of Thermal Sciences 209 (2025) 109515

Contents lists available at ScienceDirect

International Journal of Thermal Sciences

journal homepage: www.elsevier.com/locate/ijts

Experimental investigation of heat transfer, thermal efficiency, pressure drop, and flow characteristics of Fe_3O_4-MgO magnetic hybrid nanofluid in transitional flow regimes

Victor O. Adogbeji [a], Mohsen Sharifpur [a,b,c,*], Josua P. Meyer [a,d]

[a] Department of Mechanical and Aeronautical Engineering, University of Pretoria, Pretoria, Private Bag X20, Hatfield, 0028, South Africa
[b] School of Mechanical, Industrial and Aeronautical Engineering, University of the Witwatersrand, Private Bag 3, Wits, 2050, South Africa
[c] Department of Medical Research, China Medical University Hospital, China Medical University, Taichung, Taiwan
[d] Department of Mechanical and Mechatronic Engineering, Stellenbosch University, Stellenbosch, South Africa

ARTICLE INFO

Keywords:
MHNFs
Nanofluid
Nanoparticle dispersion
Pressure drop
Transition flow
Turbulence suppression

ABSTRACT

This study investigates the heat transfer characteristics of Fe_3O_4-MgO/DIW Magnetic Hybrid Nanofluids (MHNFs) compared to deionized water (DIW) across turbulent, laminar and transition flow regimes. Results reveal that the transition of MHNFs begins at significantly higher Reynolds numbers than DIW, contradicting previous findings. This disparity may be due to the specific characteristics of MHNFs, such as altered thermal conductivity and viscosity. Heat transfer results demonstrate enhancement within the fully developed transition regime, with improvements observed for MHNF concentrations from 0.3 to 0.00625 vol%. Volume fraction significantly impacts nanofluids' convective heat transfer characteristics, with higher volume fractions corresponding to higher critical Reynolds numbers. Even at 0.00625 % vol, the transition begins at a lower Reynolds number than DIW. The maximum enhancements in heat transfer were 26 % for 0.3 vol%, 25.8 % for 0.2 vol%, 25.7 % for 0.1 vol%, 17.9 % for 0.05 vol%, 25.6 % for 0.025 vol%, 31.6 % for 0.0125 vol%, and 30.2 % for 0.00625 vol% MHNFs. The optimum enhancement was observed with MHNF concentrations of 0.0125 vol% and 0.00625 vol%. Higher volume fractions led to increased pressure drops, indicating a complex interplay between fluid dynamics and nanofluid properties. The study highlights notable enhancements in thermal efficiency across transition and laminar flow regimes.

1. Introduction

Due to growing requirements for enhancing heat exchanger efficiency, novel heat transfer fluids known as nanofluids emerged in the late 20th century. The concept of nanofluids was initially coined by Choi in 1995 [1]. Sparking investigations into various nanoparticles like Fe_3O_4, Si O_2, CNT, MCNT, CuO, Al_2O_3, and Ti O_2 to enhance convective heat transfer (CHT) by altering thermal properties and fluid behavior [2–4]. Researchers are now exploring a unique category of nanofluids by integrating magnetic particles such as nickel, iron, and cobalt into standard working fluids [5,6]. Ferrofluids, comprising nanoscale magnetic particles dispersed in a carrier liquid, commonly utilize iron oxides like Fe_2O_3 (hematite) and Fe_3O_4 (magnetite). In the realm of convective heat transfer, magnetic hybrid nanofluids (MHNFs) have garnered significant interest because their potential for enhancing heat transfer rates. MHNFs have emerged as promising candidates for various thermal applications due to their unique properties and tunability. Previous studies have primarily focused on examining the effects of magnetic fields on convective heat transfer in laminar and turbulent flow regimes using single nanofluids. Since 1883, research attention has been devoted to fluid flow within tubes, particularly in understanding laminar and turbulent flow dynamics. However, it wasn't until 1990 that Professor Ghajar and colleagues pioneered research into transitional flow phases within tubes [7]. Despite extensive research following Professor Ghajar's work [7], inlet configuration and pressure drop [8], constant wall heat flux flow regime map and inlet configuration [9], correlation in transition [10], and inlet geometry effect on full developed frictional factor [11] etc, only a few researchers have experimentally investigated this region because the transitional flow region is distinguished by oscillations between laminar and turbulent behaviors., remains relatively

* Corresponding author. Department of Mechanical and Aeronautical Engineering, University of Pretoria, Pretoria, Private Bag X20, Hatfield, 0028, South Africa.
E-mail address: mohsen.sharifpur@up.ac.za (M. Sharifpur).

https://doi.org/10.1016/j.ijthermalsci.2024.109515
Received 5 June 2024; Received in revised form 5 October 2024; Accepted 4 November 2024
Available online 19 November 2024

unexplored in this context Nagendra et al. [12]. For instance, Meyer and Olivier [13], explored the impact of inlet configurations on transition heat transfer and pressure drop in smooth horizontal tubes. Meyer and Olivier [14] also nvestigated the transitional regime's friction factor with four different inlet configurations for enhanced tubes. Furthermore, Meyer and Olivier [14] studied diabatic flow in enhanced tubes with various inlet types. Everts and Meyer [15] collected heat transfer and pressure drop data under constant heat flux for both fully and developing flows in the transitional flow regime. In parallel, Meyer, and Everts [16] investigated mixed convection laminar flow and its influence on transition, developing correlations to describe the relationship between heat transfer, pressure drop, and flow regimes, including transition. They also presented flow regime maps covering both fully developed and developing flows [17]. In 2019, Osman et al. [18] investigated the impact of boundary layer chopping at the inlet on transition heat transfer and pressure drop characteristics in smooth horizontal tubes. However, while the above-mentioned works primarily focused on water, only a few research studies have concentrated on nanofluids in the transitional region. Lee et al. [19] examined the impact of a magnetic flux on forced convective heat exchange properties of various nanofluids, including, EG-based/ Fe_3O_4 nanofluids, water and Fe_3O_4/MWCNT hybrid nanofluids. The experiments covered a Re of 1000–1600 and nanoparticle volumetric ratio spanning 0.025 %–0.2 %. Their observations revealed the highest convective heat exchange efficiency of MWNCT nanofluids, with enhancements of 3.23 % and 2.78 % observed for MWNCT nanofluids containing 0.1 wt% Fe_3O_4 and 0.2 wt% Fe_3O_4, respectively. Furthermore, they observed an uptick in the typical pressure drop, with increments of 4.73 % and 5.23 % observed for nanofluids containing 0.2 wt% Fe_3O_4 and 0.2 wt% Fe_3O_4/MWNCT, respectively.

Selimefedigil et al. [20] investigated phase transition dynamics in encapsulated phase change materials (PCM) using magnetic fields and wavy conductive walls during hybrid nanofluid convection. They varied Reynolds numbers (Re), magnetic field strengths (Ha), wavy wall amplitudes (Af), wave numbers (Nf), and conductivity ratios (Kr) with a 2 % solid volume fraction of binary nanoparticles. Their results showed a reduction in phase transition time (PT) by up to 46.7 % with flat walls and 22.5 % with wavy walls, with the magnetic field improving performance. Wavy walls reduced PT further by about 9 % at the highest magnetic field strength. Key factors influencing PT included corrugation amplitude and wave number, with a 30 % variation in PT observed. Higher conductivity ratios also decreased PT by up to 42.3 %. Optimal parameters for phase transition were identified as (Ha, Af, Kr) = (30, 0.067, 2.7) at Re = 100 and (30, 0.007, 1.30) at Re = 500.

Talebi et al. [21] conducted a study to investigate forced convection using nanofluids containing Cu, Fe_3O_4 and Cu/ Fe_3O_4 hybrid nanoparticles. They examined three different volume fractions (1 %–4 %.) and three Reynolds numbers (600, 1200, 1800) to determine the local Nusselt number. Their findings indicated that both single and hybrid nanoparticles led to an improvement in heat exchange efficiency. This increment was noticed to have been imparted by both the Re and nanoparticles volume fraction. In addition, they noticed that the heat exchange improvement was pronounced on the hybrid nanofluid, with an enhancement of 11.9 % more than on Cu/water, with an enhancement of 7.8 %. Sundar et al. [22] in an experiment with Fe_3O_4 magnetic nanofluids in vacuum pump oil under laminar flow, thermal conductivity improved by 9 % at 0.5 % volume concentration. Viscosity increased 1.75 times at 60 °C. Convective heat transfer rose by 13.1 % and 17.8 %, and the *Nu* increased by 13.48 % and 8.95 % for mass flow rates of 0.208 kg/s and 0.0416 kg/s. However, this improvement led to a 1.21 times higher friction factor when evaluated alongside the base liquid.

Shahsavar et al. [23] investigated a study to determine the impact of a magnetic field on CHT using a Fe_3O_4/CNT. They investigated the impact of alternating and constant magnetic flux. Their observations showed a substantial enhancement in convective heat exchange with no magnetic flux, with the highest increase of 62.7 % in the local *Nu* observed for hybrid nanofluids concentrations exceeding 1.35 vol% CNT and 0.5 vol% Fe_3O_4 at a Re of 2190. Additionally, they noticed that the heat exchange of the hybrid nanofluid was enhanced when subjected to a continuous magnetic flux in contrast to a variable magnetic field. Furthermore, they found that higher volume fractions and lower Re led to higher enhancements in heat exchange in the hybrid nanofluids, with the highest increase reaching 20.5 % compared to without a magnetic field.

Selimefedigil and Oztop [24] investigated a phase change process in a channel with double rotating circular cylinders and a phase change material-packed bed (PCM-PB) under a magnetic field. They used finite element analysis to explore the combined effects of magnetic fields and rotations on the PCM-PB system's phase change and thermal performance. Their results indicate that magnetic field effects significantly impact vortex redistribution within the PCM-PB zone, leading to vortex suppression. At the highest magnetic field strength and a Reynolds number of −1000, the temperature coefficient (tC) was reduced by up to 74 %. The hybrid nanofluid with PCM configuration achieved the highest heat transfer rates despite the presence of magnetic field effects.

Askari et al. [25] studied the CHT of a Fe_3O_4/graphene magnetic hybrid flowing through a straight horizontal tube in a turbulent flow regime with different volume concentrations. They noticed an increment in thermal conductivity by 14–32 % for 1 % volume fraction for Fe_3O_4 and Fe_3O_4/graphene nanofluids at 20 and 40 °C opposed to base liquids with the same parameters at a Re of 4248, also the increased the CHT transfer coefficient of Fe_3O_4 and Fe_3O_4/graphene nanofluids to about 8.5 % and 14.5 %, respectively.

Sundar et al. [26] examined CHT and friction factor in turbulent flows of MWCNT-Fe_3O_4/water with a constant heat flux and orrelation was suggested to compare the *Nu* and friction factor against the experimental data for predictive purposes. Their results verified that a maximum 31.10 % increase in *Nu* was observed with a penalty of 1.18, and this compared to a 0.3 % increase in pumping power for particle loading at a Re of 22,000 the same parameters led to the use of the base liquid. They presented the following correlation. In 2015, Aghabozorg [27]. examined the effect of Fe_2O_3-CNT in a horizontal shell and tube heat exchanger under turbulent and laminar, transient, flow conditions with three different heat fluxes. They utilized Fe_2O_3-CNT of 30 nm nanoparticles diameter dispersed in DI. They aimed to examine the impact of temperatures and concentration on CHT. Increasing concentrations and temperatures led to improved CHT. Results showed that Fe_2O_3-CNT nanofluids had higher heat transfer coefficients justaposed to the base liquid, with enhancements of 13.54 % and 27.69 % for laminar and turbulent flow at 0.1 % concentration, and 34.02 % and 37.50 % for laminar and turbulent flow at 0.2 % concentration, respectively. was improved. Chougule and Sahu [28] conducted experiments on the CHT of CNT/ H_2O and Al_2O_3/ H_2O nanofluids using helically twisted tape inserts in a horizontal round tube. They varied volume fraction (0.15 %, 0.45 %, 0.60 %, and 1 %) and twist ratios (TR) of the helical tape inserts (1.5, 2.5, and 3). Results showed higher thermal efficiency for CNT/ H_2O nanofluids compared to Al_2O_3/ H_2O nanofluids. highest heat exchange improvement was seen with CNT/ H_2O nanofluid (1 %) and helical screw tape inserts with a twist ratio of 1.5. Osman et al. (2019) [29] examined CHT of Al_2O_3/ H_2O nanofluids in a rectangular channel. They tested nanofluids with volumetric fractions of 0.3 %, 0.5 %, and 1 % across Reynolds numbers of 200–7,000, covering laminar, turbulent, and transitional flows. Significant improvedment in heat exchange coefficients were noticed, particularly with the 1.0 % nanofluid showing a 54 % improvement in the transition flow regime and an 11 % increase in the turbulent regime. The transition flow regime exhibited better CHT efficiency compared to turbulent and laminar flow regimes. Meyer et al. (2013) [30] experimented with MWCNT-water nanofluids in a straight horizontal circular tube to study CHT in the transition region. They tested nanofluid concentrations (0.33 %, 0.75 %, and 1 %) across Reynolds numbers from 1,000 to 8,

000. Transition onset was earlier with higher nanofluid concentrations. Although no increase in heat transfer coefficients was observed compared to H_2O, Nusselt numbers showed enhancement due to increased nanofluid viscosity compared to thermal conductivity. In 2023, Ibrahim et al. [30] studied the entropy and exergy properties of Al_2O_3-MWCNT hybrid nanofluids in transitional flow. They varied particle sizes and concentrations, observing the best performance with specific size combinations. Their findings revealed reductions in frictional and thermal entropy, particularly in transitional and turbulent flows, showing an exergy efficiency of 54.12 % at Re 4500 and 47.85 % in transitional flow. In this regime, reductions of 6.78 % and 13.53 % in frictional and thermal entropy, respectively, were noted compared to Al_2O_3 (5 nm) - MWCNT (<7 nm) nanofluids. In turbulent flow, entropy effects were reduced by 16.66 % and 24.7 %, respectively.

In another study by Ibrahim et al. [31] explored the influence of varied particle sizes on the heat transfer properties of hybrid nanofluids within the transitional flow regime. The study utilized four distinct nanoparticle sizes to formulate nanofluids composed of Al_2O_3 and MWCNT nanoparticles (<7 nm and 30–50 nm for MWCNT, and 5 nm and 20 nm for Al_2O_3). The researchers utilized a weight ratio of 60:40 and formulated a 0.3 % volume concentration from various combinations of nanoparticles. The findings revealed that nanoparticle size significantly affects the CHT properties of the nanofluids. Each fluid exhibited different critical Reynolds numbers in the transition region. The combination of Al_2O_3 (20 nm) and MWCNT (<7 nm) demonstrated the best heat transfer performance, achieving a *Nu* increase of approximately 48.86 % in the transitional flow. This combination also had a superior coefficient of thermal performance, with improvements of 43.53 % and 21.89 % compared to Al_2O_3 (20 nm) – MWCNT (30–50 nm) and Al_2O_3 (5 nm) – MWCNT (<7 nm) nanofluids, respectively. Additionally, its pressure drop and friction factor were lower by 12.78 % and 5.2 % opposed to the Al_2O_3 (5 nm) – MWCNT (<7 nm) nanofluid. The study concluded that nanoparticle size impacts the heat transfer and flow properties of Al_2O_3 and MWCNT hybrid nanofluids at a 60:40 wt ratio.

Despite indications of improved heat transfer in the transitional region, particularly noted in previous studies, there remains a notable scarcity of research focused on hybrid nanofluids, especially MHNFs, within this domain. Consequently, this study addresses this research gap by delving into the performance of MHNFs, specifically within the transitional flow regime. Through this investigation, we aim to provide a more comprehensive understanding of the heat transfer properties of MHNFs in transitional flow conditions, thereby contributing valuable insights to the existing body of knowledge.

The choice of Fe_3O_4 (Magnetite) and MgO (Magnesium Oxide) as nanoparticles for this study is grounded in their distinct yet complementary properties, which are crucial for optimizing the heat transfer performance and stability of MHNFs. Specifically, MgO was chosen for its superior thermal conductivity and chemical stability, both of which are critical in enhancing heat dissipation and maintaining nanofluid performance under varying conditions. MgO's high thermal conductivity ensures efficient heat transfer, particularly important in thermal management applications, while its chemical resilience and high melting point allow it to function effectively in high-temperature environments without degradation. Its low density also helps minimize increases in viscosity, reducing the pumping power required to circulate the nanofluid an important consideration in energy efficiency.

Fe_3O_4, on the other hand, was selected for its exceptional magnetic properties. These allow the MHNFs to respond to external magnetic fields, improving nanoparticle dispersion, preventing agglomeration, and influencing flow structures, all of which contribute to better heat transfer. Additionally, Fe_3O_4 has moderate thermal conductivity and high magnetic susceptibility, enhancing heat transfer when exposed to a magnetic field. Its superparamagnetic behavior ensures that the nanoparticles do not retain magnetism once the magnetic field is removed, reducing the risk of particle aggregation over time.

The combination of MgO's thermal efficiency and Fe_3O_4's magnetic controllability creates a hybrid system optimized for both heat transfer and stability across various flow regimes, including the transitional regime. This study specifically addresses a gap in the existing literature, where most research has focused on single-component nanofluids like Fe_3O_4 or densely packed oxide nanoparticles, which can increase fluid viscosity and lead to higher energy requirements for pumping. In contrast, this study explores the use of MHNFs in the transition flow regime, a relatively under-explored area.

Additionally, existing studies have shown that nanoparticle size and volume fractions can notably influence the onset and end of the transition flow regime and heat transfer performance. By exploring the effect of different volume fractions of Fe_3O_4-MgO MHNFs on the start and end of the transition regime, this study aims to offer new insights into the heat transfer, thermal efficiency, pressure drop, and flow characteristics within the transitional flow region. This focus on the impact of nanoparticle concentration further aligns with the study's goal of identifying the optimal conditions for improved thermal performance.

Therefore, MgO and Fe_3O_4 were selected based on their synergistic properties Mof MgO for thermal conductivity and Fe sub 3, O sub 4for magnetic control, which offer enhanced heat transfer and stability. The study aims to fill a critical gap in understanding the behavior of MHNFs in transitional flow, particularly how nanoparticle volume fractions affect the transition regime because existing research indicates that multiple variables impact the onset and conclusion of the transition regime. However, there is a notable absence of studies examining the factors influencing these transitions, specifically using nanofluids, especially MHNFs nanofluids. Similarly, the influence of varying volume fractions on initiating and completing the transition regime within a tube has not been extensively explored. In contrast, numerous studies have extensively documented the initiation of the transition regime in tube flows employing water as the working fluid.

However, Ibrahim et al. [31] examined the impact of particle size using four different particle sizes of nanofluids composed of MWCNT and Al_2O_3 (i.e., 5 nm and 20 nm for Al_2O_3 and <7 nm and 30–50 nm for MWCNT) with a 0.3 % volume fraction and a ratio of 60:40. They explained that transition is influenced by several factors. Their findings indicated that particle sizes had a notable effect on the CHT properties of nanofluids throughout the transition region and at the onset and conclusion of the transition. The introduction of nanoparticles into the base fluid could influence the initiation of transitional flow. This study aims to investigate the effect of different volume fractions using MHNFs to determine the start and end of the transition regime. Additionally, we will examine the impact on the heat transfer, thermal efficiency, pressure drop, and flow characteristics of Fe_3O_4-MgO Magnetic Hybrid Nanofluid in transitional flow regimes.

2. Nanofluids materials and preparation

In this study, MHNFs of Fe_3O_4 and MgO dispersed in DIW were prepared with a two-step technique, yielding the targeted concentration ranging from 0.00625 vol% to 0.3 vol%.The respective Iron III Oxide Fe_3O_4 nanoparticles and Magnesium Oxide (MgO) with a hybridization mixing ratio (HMR) 0f 80:20 was considered, and the properties of the MHNFs are shown in Table 1. The nanoparticles, dispersant, and water mixture underwent mechanical stirring by hand followed by ultrasonication for 4 h using a Qsonica (Q-700) sonicator set to 100 % sonication amplitude within a constant bath temperature set at 20 °C. Physical observations and viscosity measurements over time at around 30 °C were monitored for approximately 5 h. The stability of the nanofluids was evaluated using a methodology similar to previous research conducted by Giwa et al. [32], and Osman et al. [29]. The result in Fig. 1(a) shows the physical observation of the ferrofluid after over 24 h of preparation, while Fig. 1(b) shows the viscosity of the respective sample of the Fe_3O_4-MgO/water ferrofluid. The viscosity value over this time interval shows that the nanofluids is slightly stable.

Table 1
Detail chart of MHNFs particles used.

Properties	Deionized water (DIW)	Iron (III) oxide(20–30 nm)	Magnesium Oxide MgO (20–40 nm)	Dispersant
Density (kg/m^3)	997	5100	3580	Gum Arabic
Thermal conductivity (W/m.k)	0.613	80.2	43	
Specific Heat capacity (J/kg.k)	4179	670	903	
Shape	–	Plate-like nanosheet	spherical	Sigma-Aldrich, Germany
Supplier		Nanostructured and Amorphous Material Inc., USA	Nanostructured and Amorphous Material Inc., USA	

Source: Material Data sheets from Nano Research Materials Inc. (USA) (US4314)

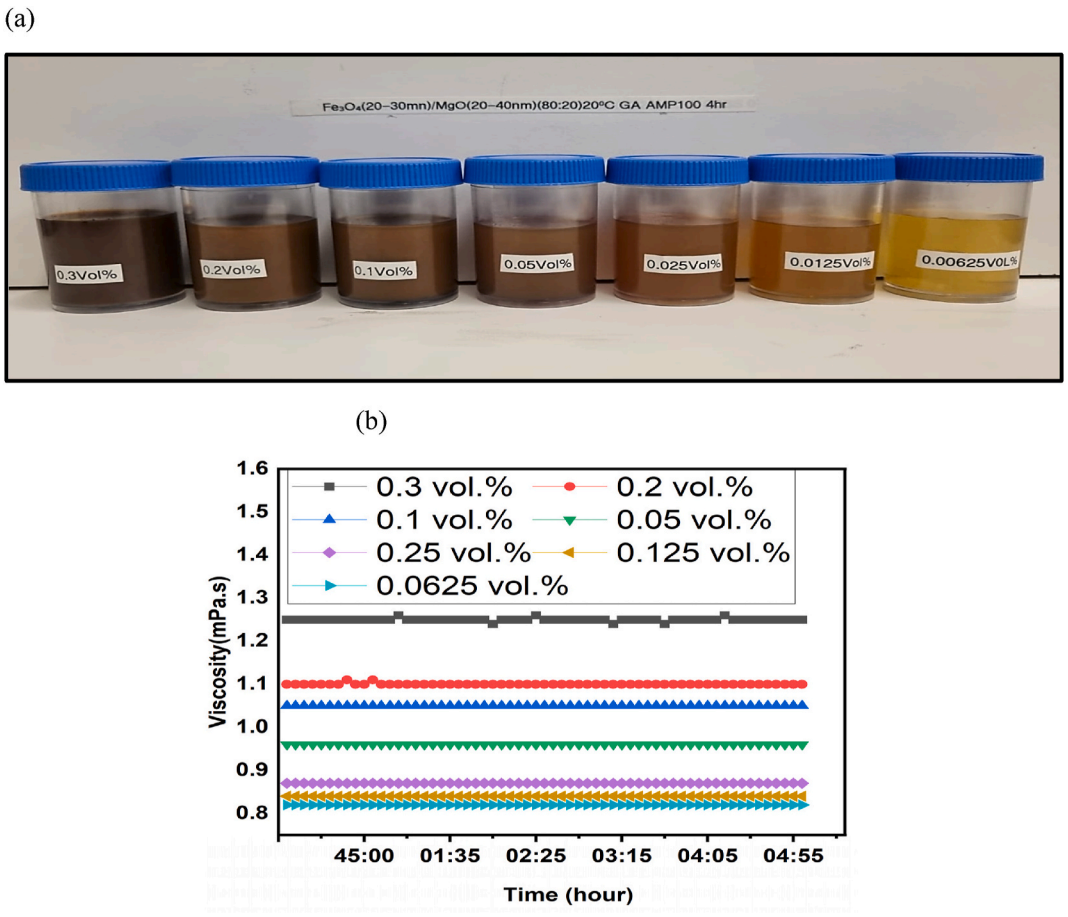

Fig. 1. Stability of the MHNFs (a) Physical Inspection (b) Viscosity over time at 30°C.

2.1. Nanoparticle's morphology

A comprehensive analysis of the morphologies of Fe_3O_4 and MgO nanoparticles was conducted using a Zeiss Crossbeam 540 scanning field emission gun electron microscope (FEG-SEM) at the Microscopy Department of the University of Pretoria. Before visualization in the FEG-SEM, meticulous preparation of the nanoparticle samples was undertaken, resulting in the generation of the images presented in Fig. 2. Upon inspection of the Fe_3O_4 nanoparticles image, a spherical morphology with blade-like particle clusters was observed. Conversely, the MgO nanoparticles image displayed a uniformly spherical shape with no particle clustering. Interestingly, the hybrid nanoparticle image revealed that MgO particles adhered to the edges of the blade-like clustered Fe_3O_4 particles. This observation suggests that the hybridization could potentially enhance thermophoretic forces within the liquid upon dispersion, thereby contributing to improved electro- and thermophoretic behavior in the fluid when subjected to electrical and thermal forces. These findings align with existing literature on nanoparticle morphology, providing further validation for the accurate identification of the nanoparticles as indicated by the manufacturer.

2.2. UV–visible spectrophotometry for stability check

The stability of MHNFs was evaluated using UV–Visible spectroscopy with an ONDA TOUCH UV-21 Spectrophotometer at ambient temperature, with deionized water (DIW) as the reference. Each sample was measured six times, and the average values were recorded. The light spectrum ranged from 200 to 300 nm, with 10 nm intervals from 200 to 280 nm, and 1 nm intervals between 281 and 300 nm for all samples. The absorbance at various wavelengths and the sedimentation percentage of MHNFs were calculated using Equation (2).

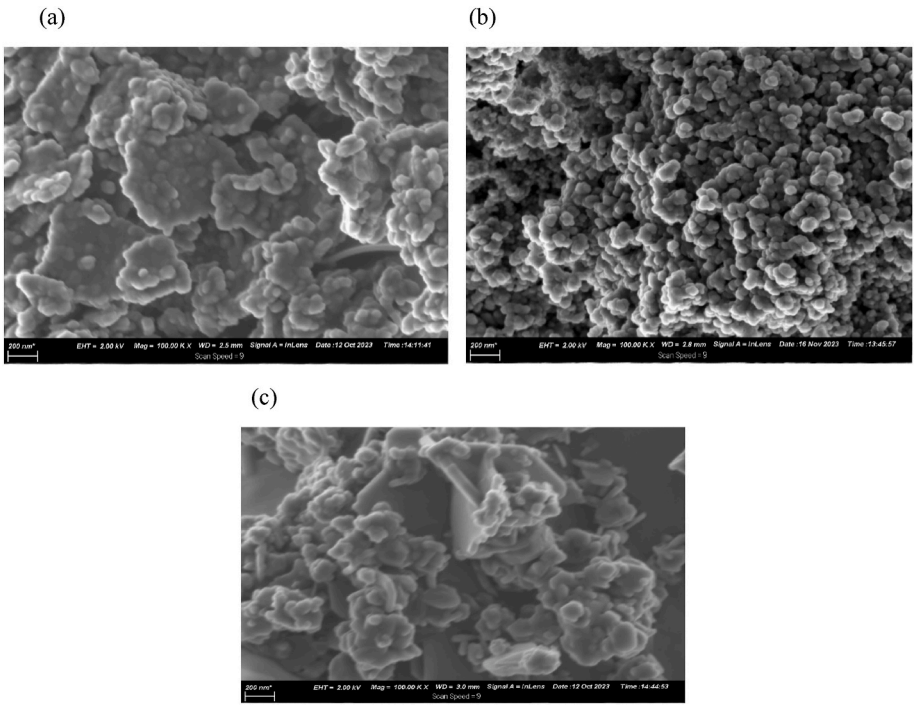

Fig. 2. SEM images of (a) Fe_3O_4 [20–30 nm], (b) MgO [20–40 nm] and (c) Fe_3O_4-MgO hybrid.

$$\text{Percentage (SF)} = \left(\frac{\textit{Total Sedimentation factor}}{\text{Total Maximum absorbance}}\right) \times 100 \quad (2)$$

UV–Vis spectroscopy, in accordance with Beer-Lambert's law [33, 34] demonstrated a UV–Vis spectroscopy demonstrated a clear correlation between the absorption rates of Fe_3O_4/MgO nanofluids and their particle volumetric fractions, as depicted in Fig. 3. Chakraborty et al. [35], findings suggest that the stability of nanofluids can be quantitatively evaluated through spectral absorbance and transmittance measurements. This method, particularly effective for tracking nanofluid stability, involves monitoring changes in absorbance over time using UV–visible spectroscopy. A decline in absorbance indicates instability, reflecting nanoparticles' propensity to settle out of the suspension.

In this study, the sedimentation percentages for Fe_3O_4/MgO nanofluids at various volume fractions revealed a consistent trend where higher concentrations led to increased sedimentation. Specifically, sedimentation percentages were recorded as 11.53 % for 0.3 vol%, 11.23 % for 0.2 vol%, 10.7 % for 0.1 vol%, 10.3 % for 0.05 vol%, 9.0 % for 0.025 vol%, 8.7 % for 0.0125 vol%, and 8.0 % for 0.00625 vol%. This data indicates that nanofluid stability decreases with increasing nanoparticle concentration, as higher volume fractions correspond to greater sedimentation rates.

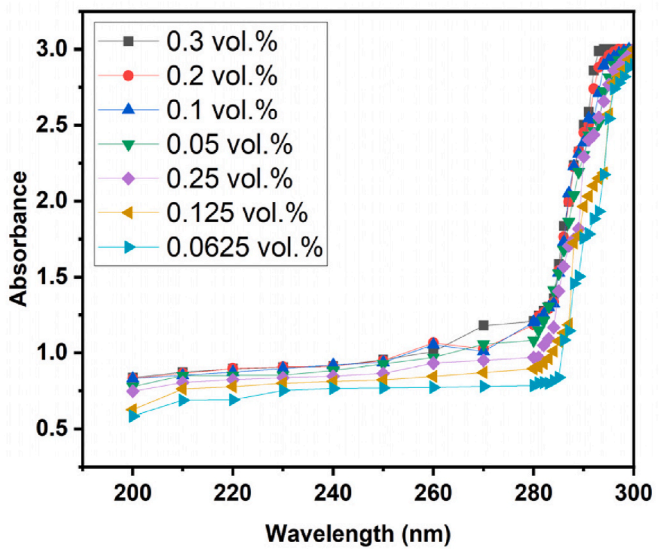

Fig. 3. Impact of Fe_3O_4/MgO/DIW density on light absorption at different wavelength for stability check.

The pH values of the nanofluids, measured at a constant room temperature of 25 °C, remained relatively stable across all volume fractions. The values stayed within a basic range, inhibiting particle aggregation and contributing to stability. However, despite the favorable pH conditions, the observed sedimentation trend suggests that increased nanoparticle concentration compromises the overall stability. While the basic pH environment mitigates some particle aggregation, it does not fully counteract the instability caused by higher concentrations of nanoparticles.

The study's findings highlight the need to consider both pH levels and nanoparticle concentration when managing nanofluid stability. Although maintaining a basic pH can help reduce particle aggregation, the increase in sedimentation at higher concentrations reveals a challenge in preserving stability. This underscores the necessity for careful optimization, including the possible use of stabilizers, particularly at higher nanoparticle concentrations, to ensure consistent performance.

The UV–Vis spectroscopy results further demonstrate that lower absorption rates are directly linked to reduced particle volumetric fractions, which correspond to lower sedimentation percentages. Over a 30-day observation period, significant settling was detected in nanofluids with volume fractions of 0.3 %, 0.2 %, and 0.1 %, with sedimentation factor (SF) percentages of 11.53 %, 11.23 %, and 10.7 %, respectively. In contrast, nanofluids with smaller volume fractions of 0.00625 %, 0.0125 %, and 0.025 % exhibited greater stability, with SF percentages of 9.0 %, 8.7 %, and 8.0 %, respectively. This reflects their commendable stability, while nanofluids with 0.05 % volume fraction displayed moderate stability. The results suggest that nanofluids with higher concentrations 0.1 %, 0.2 %, and 0.3 % are less stable, indicating a need for optimization and the use of stabilizers to enhance their

stability at higher concentrations.

2.3. Thermophysical properties measurement

The thermal conductivity and viscosity of fluids of Fe_3O_4-MgO/water ferrofluid were determined using the instrumentations and methodology outlined by Ref. [36]. The viscometer underwent calibration using a single-point standard calibration method with DIW. Afterwards, the measured viscosity of water for the temperature range of 10°C–50°C was compared to values reported by Senger & Watson [37]. Then, viscosity readings were obtained for various MHNFs. The results, illustrated in Fig. 4(a), there is a clear and consistent trend indicating a reduction in fluid viscosity as the temperature increases across all samples, including de-ionized water. Interestingly, it was observed that the ferrofluid samples with a volume fraction of 0.00625 % exhibited marginally elevated viscosity compared to DIW. Among the volume fraction, however 0.3 % and 0.2 % Vol showed the highest viscosity, indicating an increase in pressure drop within the system and implying the need for higher pump power.

The thermal analyzer was calibrated using a standard thermal conductivity fluid (glycerin). Subsequently, the measured thermal conductivity of DIW was taken for the temperature range 10°C–50°C and compared to values reported by Cengal et al. [38]. Thermal conductivity readings were then obtained for various Fe_3O_4-MgO/water ferrofluid samples and de-ionized water, with the results illustrated in Fig. 4(b). The findings show increased thermal conductivity with temperature, with the ferrofluid exhibiting higher thermal conductivity than de-ionized water. Among the volume fractions, 0.3 % Vol demonstrated the highest conductivity, indicating superior thermal performance compared to the other volume fractions.

To measure electrical conductivity, (a Chauvin Arnoux, C.A 10141 Instrument, France) conductivity meter was employed. Calibration was performed using a standard conductivity fluid with an average electrical conductivity of 141.36 mS/m at 25 °C. Subsequently, the electrical conductivity of the Fe_3O_4-MgO and water were measured, and the results are illustrated in Fig. 4(c). The findings showed that the ferrofluids generally exhibited significantly higher electrical conductivity than deionized water, with 0.3 % Vol displaying the peak electrical conductivity. A bench pH meter was utilized to measure pH. Calibration was conducted using standard pH buffers 7 and 10 solutions at an average

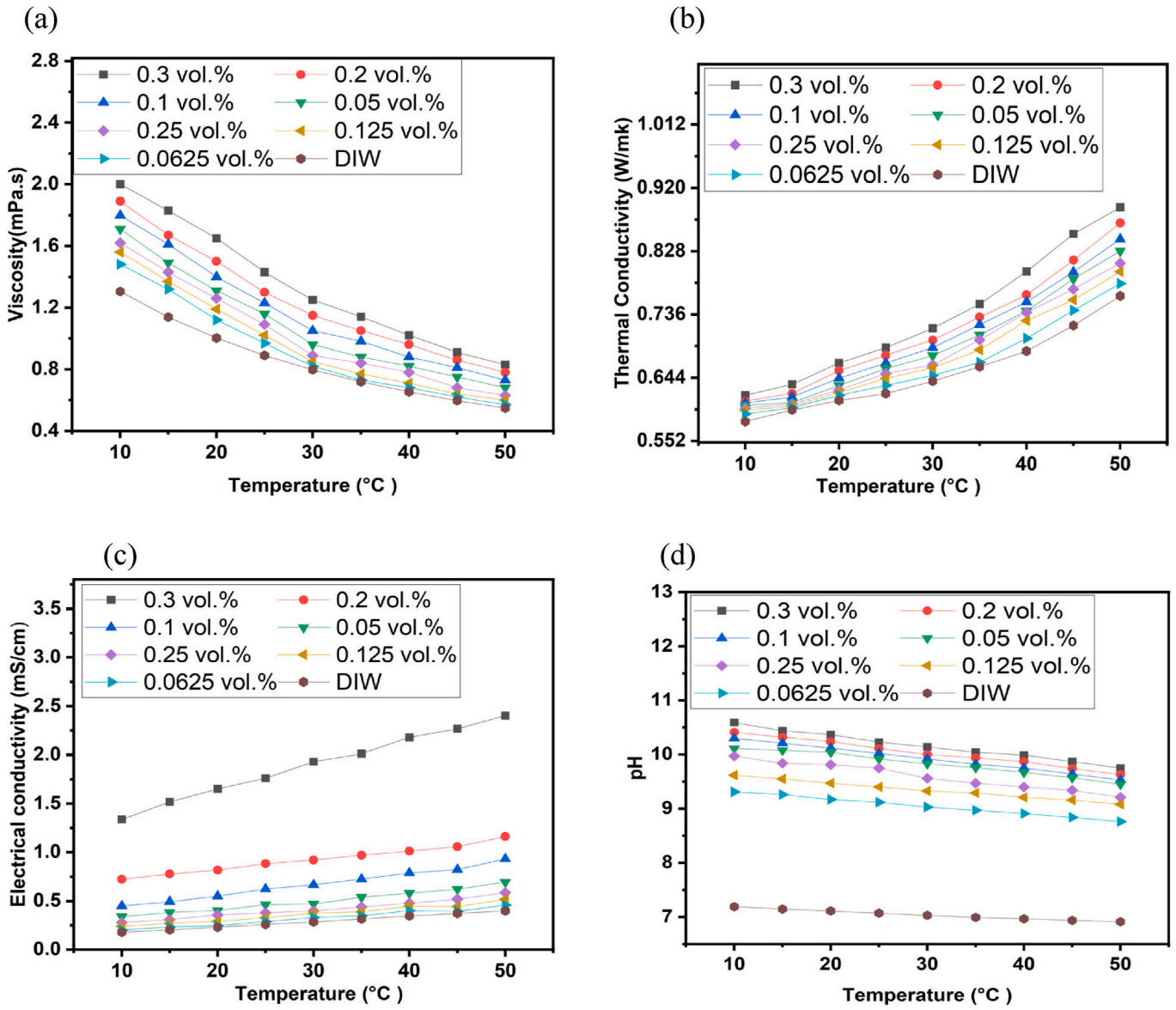

Fig. 4. Thermophysical properties MHNFs (a) Viscosity over temperature (b) Thermal conductivity over temperature (c) Electrical conductivity over temperature and (d) pH over temperature.

temperature of 25 °C. Subsequently, the pH of the Fe_3O_4-MgO and water mixture was determined, and the results are depicted in Fig. 4(d). The outcomes showed a decline in the pH levels of nanofluids with increasing temperature. Higher nanoparticle concentrations exacerbate this reduction in pH from 10.59 to 8.76, suggesting a shift from high bases to alkalis. In contrast, DIW maintains a relatively constant pH of around 7.

3. Experimental setup and methodology

Fig. 5(a) and (5b) illustrate the experimental setup and methodology for investigating forced CHT**.** The setup comprises various components, including a flow meter, a tube-in-tube heat exchanger, a DC power supply, a pressure transducer, a test section, a storage tank, a micro gear pump, thermocouples, and a data acquisition system. This setup is specifically designed to analyze the heat transfer properties of nanofluids. The test section is equipped with a Constantine heating wire wound around it to ensure controlled heating, while effective insulation is incorporated to minimize heat loss. Nanofluids with different weight concentrations are pumped through a copper pipe, and their mass flow rate is accurately measured using a flow meter. The heated nanofluids, with a constant inlet temperature of 20 °C, are then cooled through a heat exchanger, transferring heat to cold water facilitated by a circulation pump. The data acquisition system collects and processes signals from various sensors, including, flow meters, pressure transducers, the power supply and thermocouples.

In Fig. **(5c),** the test segment features a circular copper tube, 1550 mm in length, with an inner diameter of 8 mm and an outer diameter of 9.5 mm. Four thermocouples are strategically positioned to monitor tube wall temperatures at regular 130 mm intervals in the North, South, East, and West directions. Continuous temperature monitoring is conducted at both the nanofluid inlet and outlet. A 200 W Constantine wire ensures a consistent heat flux, powered by a DC source supplying 1.22 A and 180 V. To ensure fully developed hydraulics, a shorter test section measuring 1000 mm in length is used. Additionally, four strategically positioned electromagnetic locks on the test tube enable coverage of all seven thermocouples. The experiments were conducted thrice to ensure the accuracy of the data collected., and calculations are based on the average wall temperature.

The thermophysical properties of the MHNFs were evaluated, including specific heat and density, using an analytical model proposed by Pak and Cho [39], as depicted in Equations (3) and (4).

$$\rho_{nf} = (1-\varphi)\rho_{bf} + \varphi\rho_{np} \quad 3$$

$$C_{pnf} = \frac{(1+\varphi)\rho_{bf}C_{pbf} + \varphi\rho_{np}C_{pnp}}{(1-\varphi)\rho_{bf} + \varphi\rho_{np}} \quad 4$$

In these equations, φ represents the mass ratio of NF, while ρ_{nf}, ρ_{bf}, and $\varphi\rho_{np}$ and $\varphi\rho_{np}$ refer to the densities of the nanofluid, base fluid, and nanoparticles, respectively. Furthermore, C_{pnf}, C_{pbf}, and C_{pnp} indicate their respective specific heats. The determination of specific heat and density for MHNFs containing Fe_3O_4/MgO is accomplished through the application of Equations (5) and (6) [9].

To investigate CHT and *Nu* variations across different volume fractions, it is crucial to account for these thermophysical properties. This involves calculating the heat absorbed by the working fluid and the energy transferred to the test section, as detailed in Equations (7) and (8)

$$P = VI \quad 7$$

$$Q = \dot{m}c(T_O - T_i) \quad 8$$

The equation comprises numerous variables: V represents voltage, I denotes the current supplied by the power source, m and c stand for the mass flow rate and specific heat of the working fluid, respectively. T_O *and* T_i represent the outlet and inlet temperatures of the test section, respectively. Using Equation (9), calculations are evaluated to determine the local convective heat transfer coefficient along the axial distance of the test section.

$$h = \frac{Q}{A(t_w - t_b)} \quad 9$$

To compute the local CHT coefficient at each thermocouple point, the bulk fluid temperature was determined by combining the inlet and outlet temperatures with the specific heat and heat flux data obtained from a flow meter. This information was then compared with the surface temperature measured by the thermocouples, enabling the calculation of the *Nu*. The *Nu* was calculated using the convective heat transfer coefficient obtained from Equation (9) and the measured thermal conductivity of the nanofluid.

$$Nu = \frac{hD}{k} \quad 10$$

Equation (9) encompasses several parameters: A represents the area of the test section, t_w denotes the average wall temperature, t_b signifies the average bulk temperature, and *Nu* is directly linked to convective heat transfer. Additionally, D stands for the inlet diameter of the test section, and K corresponds to the thermal conductivity of the nanofluids.

The average conductive heat transfer ($h_{average}$) is determined using the local convective heat transfer coefficients measured at each thermocouple location along the test section, as described in Equation (11).

$$h_{aveg} = \frac{h_{(x1)} + \ldots\ldots\ldots\ldots\ldots\ldots\ldots h_{(xn)}}{n} \quad 11$$

Where n is equal to 7.

In addition to assessing heat transfer, the study also involved evaluating viscous pressure losses within the test section for both deionized water and nanofluids and the Colburn -j factor (j). The experimental results were then compared with predicted pressure loss and j factor is estimated from Equations (12) and (13) and Table 2.

$$f = \frac{\Delta P}{\left(\frac{L}{D}\right)\left(\frac{\rho v^2}{2}\right)} \quad 12$$

$$j = \frac{Nu}{RePr^{\frac{1}{3}}} \quad 13$$

3.1. Nusselt number validation

Before examining CHT coefficients using nanofluids, experiments were conducted with DIW Re ranging from 3000 to 10,000. To ensure the validity of our experimental setup, we validated our findings by comparing them to the equations proposed by Dittus and Boelter [40], Sieder and Tate [41], and Gnielinski [42], specifically designed for turbulent flows in Equation (14)–(16) respectively. Our experimental data exhibited strong agreement with these correlations, as demonstrated in Fig. 6. The comparison of the Dittus and Boelter and Sieder and Tate correlations with the experimental data revealed a good match in the turbulent regime. However, the Gnielinski correlation yielded even closer predictions to the experimental results. On average, it underpredicted the outcomes by less than 3 %. This validation enhances confidence in our data collection and analysis methodology, thus justifying the experimental approach, setup, and data processing techniques.

$$Nu = 0.023.\, Re^{0.8}.Pr^{0.4} \quad (14)$$

With the range of $\frac{x}{D} \geq 60, 0.7 \leq Pr \leq 120$ and $Re \geq 10,000$

$$Nu = 0.027.\, Re^{0.8}.Pr^{\frac{1}{3}}.\left(\frac{u_b}{u_w}\right)^{0.14} \quad 15$$

With the range of $0.7 \leq Pr \leq 17.600$ and $Re \geq 10,000$

(a)

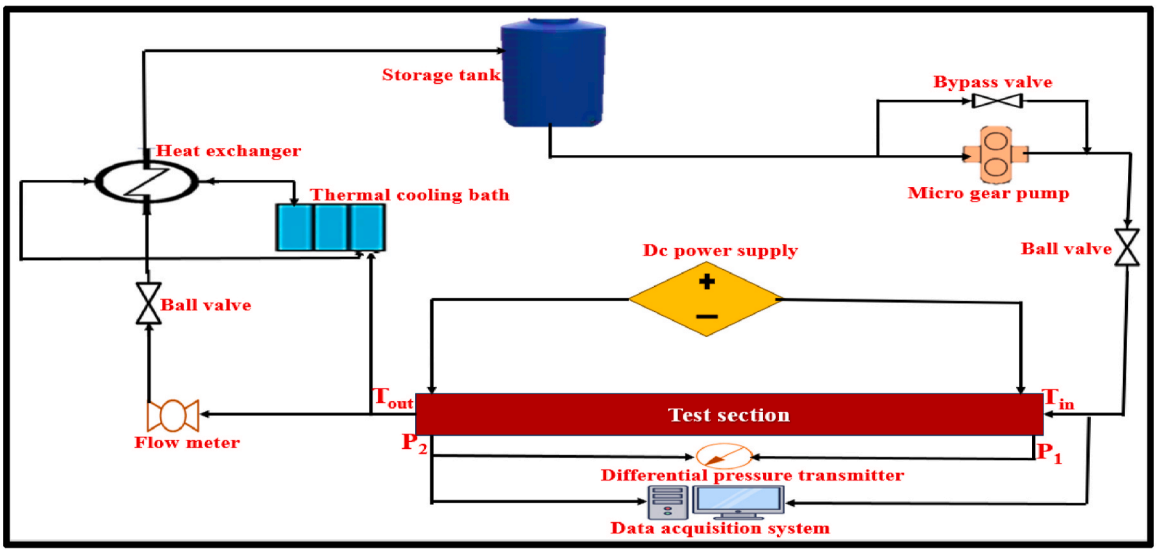

(b)

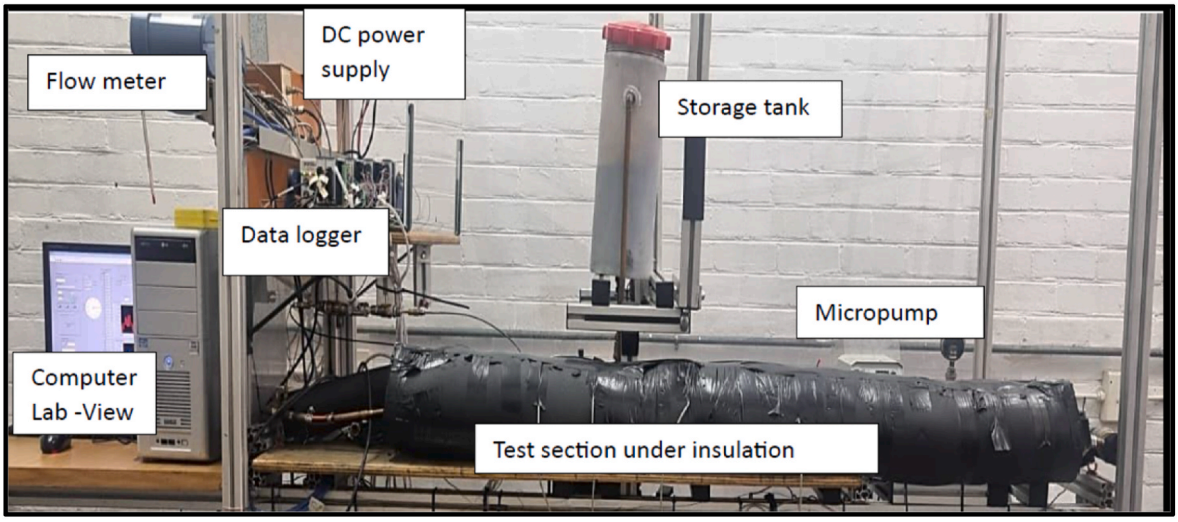

(c)

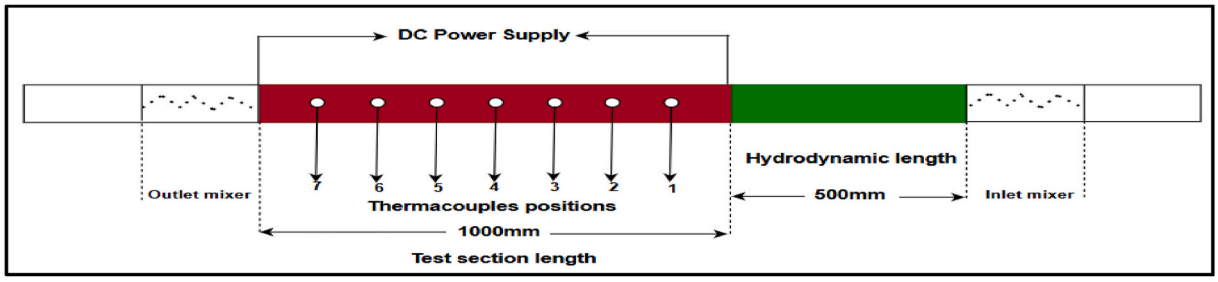

Fig. 5. Aschematic setup diagram (b) layout of the test rig (c)schematic representation of the test section for forced convective heat transfer investigation.

Table 2
Parameters used and Experimental conditions.

Parameters	Dimensional values/Ranges	Symbols
Reynold Numbers	1000–8000	Re
Heat flux	8.67kw/ m^2	$\dot{q}$
External diameter	9.5 mm	D_O
Internal diameter	8 mm	D_I
Test section length	1000 mm	L
MHNFs inlet temperature	21 °C	T_i

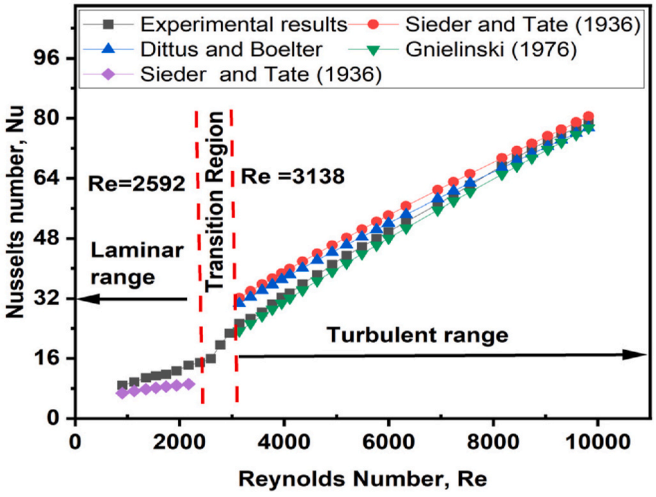

Fig. 6. Comparison between experimental data and prediction models versus Reynolds number of DIW results.

$$\mathrm{Nu} = \frac{(f/8)\,(Re - 1000)pr}{1 + 12.7\,(f/8)^{0.5}\left(pr^{\frac{2}{3}-1}\right)} \quad 16$$

$f = (0.79.ln.Re - 1.64)^{-2}$ with the range of $0.5 \le pr \le 2000$ and $3000 \le Re \le 5 \times 10^6$

3.2. Analysis of uncertainty

The methodologies recommended by Dunn [43], were utilized to determine the uncertainties of both the measured and calculated parameters, with all evaluations conducted within a 95 % confidence interval. Table 3 displays these uncertainties, which were assessed under at elevated Reynolds numbers as shown in Equation (17)–(20).

$$u_x = \sqrt{u_B^2 + U_p^2}, P\% \quad 17$$

where u_B represents bias error and u_p represents the precision error in x with a probability of P%.

The calculation of parameter uncertainty based on measured variables can be accomplished using a series of equations as outlined below in 18–20,

Table 3
Uncertainty of evaluated parameters.

Parameter	Uncertainty (%)
Reynolds number	2.145
Bulk temperature	0.727
CHT coefficient, h	2.49
Nusselt number	3.69
Δp	1.15

$$\mathrm{R}\,(x) = f(x_1, x_2, x_3, \ldots\ldots\ldots x_n) \quad 18$$

For a given variable x_i, the uncertainty in the parameter R, concerning both its mean value $\overline{R}$ and its true (actual) value R_{actual}, can be expressed as follows.,

$$R_{actual} = \overline{R} + \delta R \quad 19$$

where δR is the uncertainty in R can be expressed as follows,

$$\delta R = \sqrt{\left(\delta_{x1}\ \frac{\partial R}{\partial_{x1}}\right)^2 + \left(\delta_{x2}\ \frac{\partial R}{\partial_{x2}}\right)^2 + \ldots\ldots\ldots + \left(\delta_{x_n}\ \frac{\partial R}{\partial_{x_n}}\right)^2} \quad 20$$

Where δ_{x_i} represent the uncertainty of the evaluated variable x_i

The uncertainty of the CHT coefficient in the experimental outcomes was approximately 0.116 %, which falls well within an acceptable range. This low level of uncertainty underscores the reliability and precision of the experimental measurements, ensuring that the reported enhancements in heat transfer are both accurate and reproducible.

4. Experimental results and discussion

4.1. Impact of particle concentration on Colburn j factors

The Colburn j factor, a dimensionless parameter used to describe the convective heat transfer performance of fluids, is directly influenced by viscosity because of its role in flow dynamics and heat transfer characteristics. Viscosity affects both the frictional resistance in the fluid flow and the thermal boundary layer thickness, which in turn influences the heat transfer rate. In nanofluids, an increase in viscosity generally leads to higher frictional losses, which can negatively impact the heat transfer process by requiring more energy to maintain flow, particularly in turbulent regimes, Nagendra et al. [12], Ibrahim et al. [31] found that increased disturbances within the tube lead to an earlier onset of the transition phase. However, in some cases, the enhanced thermal conductivity of nanofluids can compensate for the increased viscosity, leading to a higher j factor. Additionally, Osman et al. [29] observed that the transition begins earlier with single nanofluids than with base fluids like water, which is attributed to the heightened fluid viscosity.

Nanofluids with the highest stability and heat transfer efficiency tend to exhibit the highest Colburn j factors because of their ability to maintain a uniform dispersion of nanoparticles over time. Stability is critical in preventing nanoparticle agglomeration, which would otherwise increase the fluid's viscosity and reduce its thermal performance by hindering effective heat transfer. When nanofluids remain stable, the nanoparticles are evenly dispersed and contribute to a more efficient heat transfer process by interacting uniformly with the base fluid.

The enhanced heat transfer efficiency in stable nanofluids is due to the improved thermal conductivity provided by well-dispersed nanoparticles, which increases the convective heat transfer coefficient. This directly raises the Colburn j factor, which is proportional to the heat transfer coefficient and inversely related to the Reynolds number. As a result, more stable nanofluids, with minimal sedimentation or agglomeration, ensure consistent and enhanced thermal conductivity throughout the flow, leading to better overall heat transfer performance and higher j factors.

Additionally, the specific surface area of nanoparticles, combined with their ability to disperse well in the base fluid, maximizes their interaction with the fluid and enhances the convective heat transfer process. Nanofluids with optimal particle concentration and stability demonstrate better heat transfer performance, reflected in higher j factors. Therefore, the highest Colburn j factors are observed in nanofluids that maintain both stability and high heat transfer efficiency, as these characteristics enable more effective thermal energy transport throughout the fluid system.

Fig. 7 (a-i) illustrates the Colburn j factor as a function of the

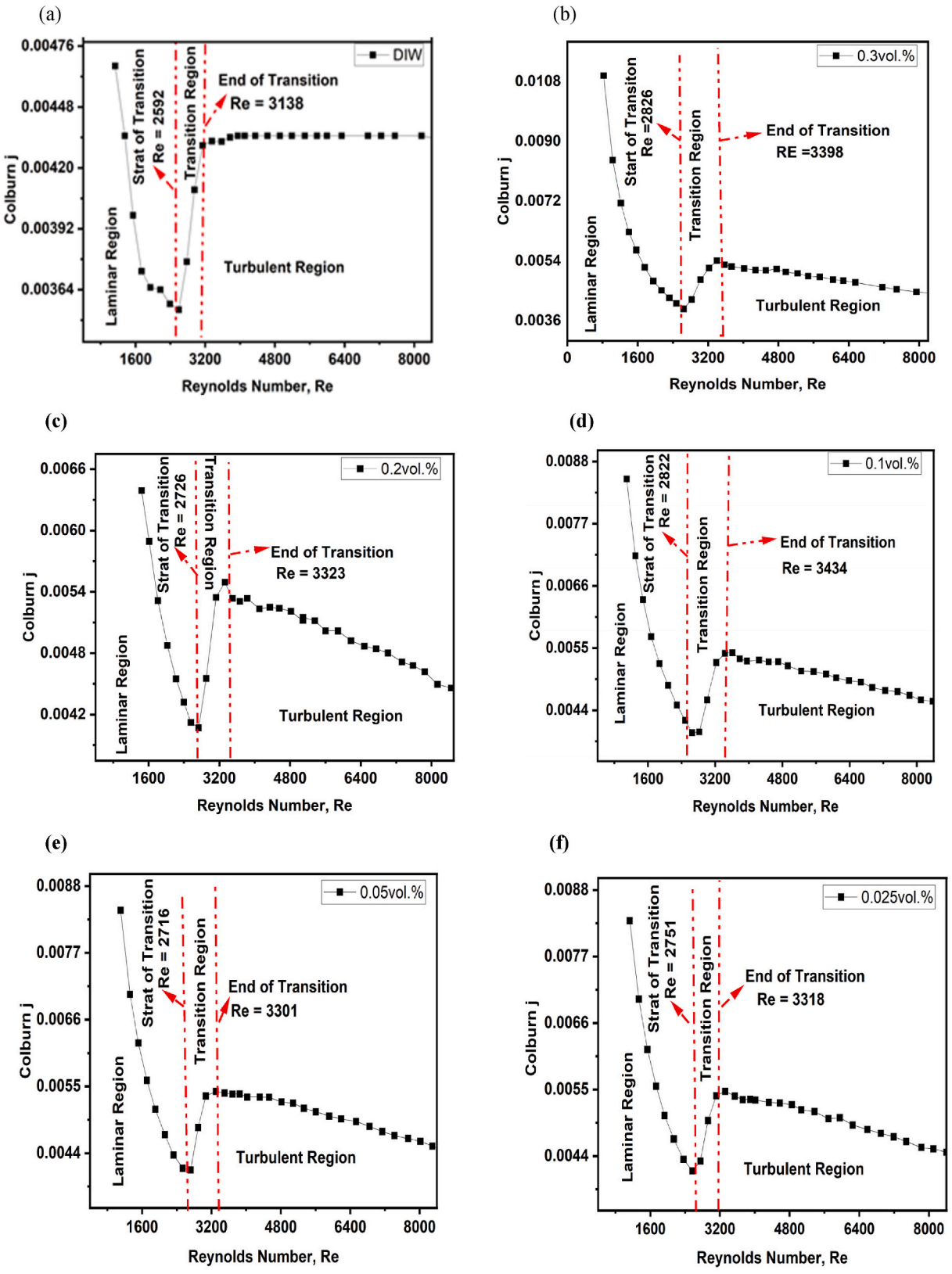

Fig. 7. Effect of Colburn j factor as a function of Reynolds number for DI water and seven different MHNFs (a) DIW, (b) 0.3 % Vol (c) 0.2%Vol (d) 0.1 % Vol (e) 0.05%Vol (f) 0.25 % Vol (g) 0.0125%Vol (h) 0.00625 % (i) Combined MHNFS samples and DIW

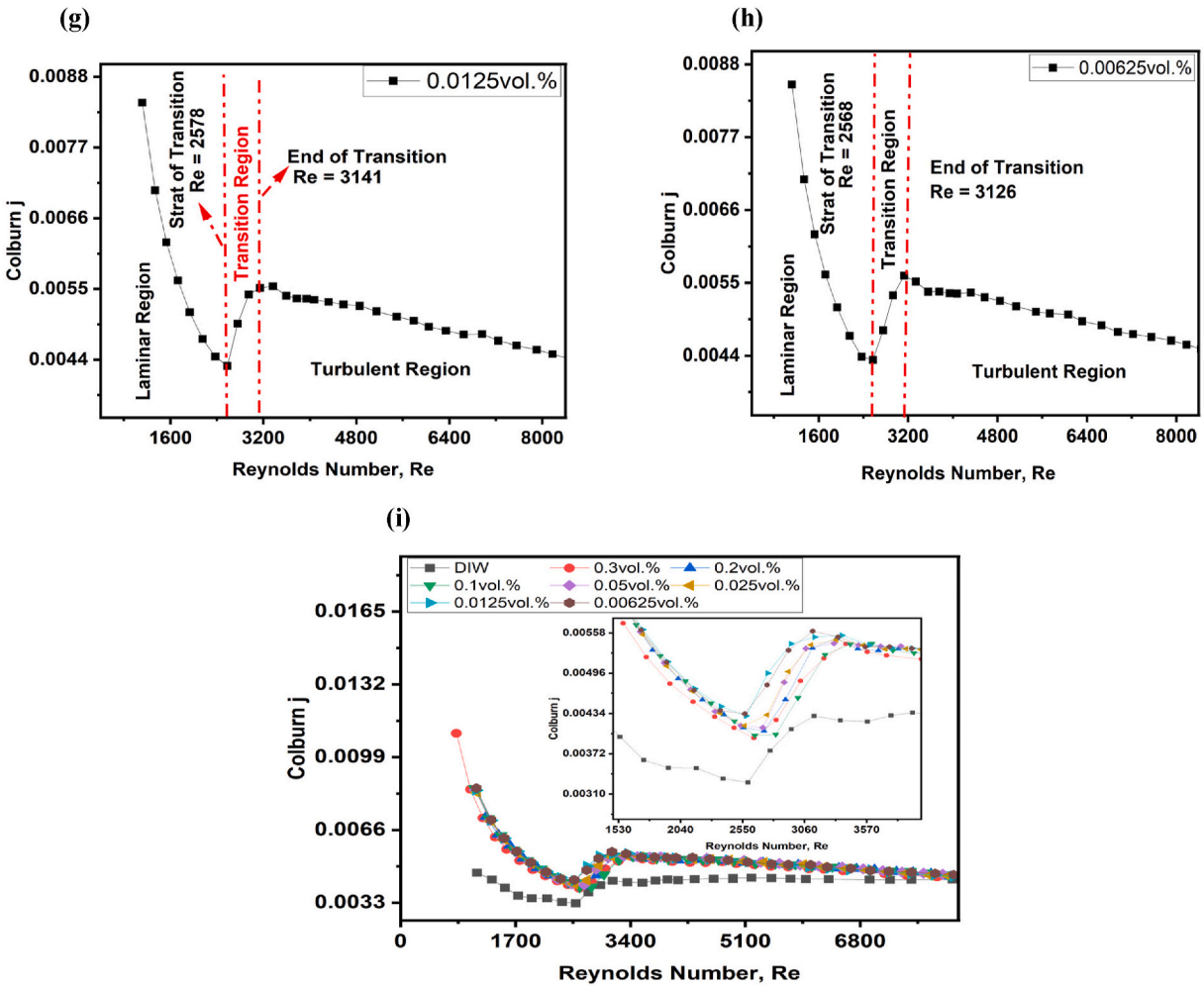

Fig. 7. (*continued*).

Reynolds number for DI water and seven different MHNFs. The graphs depict how the transitional flow regime begins at varying Reynolds numbers for different volume fractions (ranging from 0.3 % to 0.0625 %). In addition to visually representing the differences in the transition ranges among the seven fluids, the figures also demonstrate the impact of the fluids' thermophysical properties on the Colburn j factor.

The thermophysical characteristics of these MHNFs, as shown in Fig. 4, indicate that both viscosity and thermal conductivity are influenced by the particle concentration. The results reveal that the nanofluid with a 0.0125 % volume fraction has the highest Colburn j factor, followed by the 0.00625 % volume fraction. However, as the volume fraction increases from 0.025 % to 0.3 %, the Colburn j factor decreases along the transition region. Comparing this with Fig. 4, it is evident that the Colburn j factors are more significantly impacted by viscosity. This correlation is likely due to the impact of viscosity on the Prandtl number. Fig. 4 shows that the highest volume fraction corresponds to the highest viscosity, which decreases with lower volume fractions down to 0.00625 %. The Colburn j factor analysis suggests that nanofluids with the highest stability and heat transfer efficiency exhibit the highest Colburn j factors, as illustrated in Fig. 8.

Therefore, nanofluids that maintain high stability and lower viscosity at a given Reynolds number tend to achieve higher Colburn j values in the transition flow region, as shown in Fig. 7(i). In comparison to DI water, the performance of these stable nanofluids is significantly enhanced, particularly in the transition region, where the interplay between viscosity, stability, and heat transfer efficiency is most pronounced. This analysis underscores the importance of optimizing both particle concentration and fluid stability to maximize the heat transfer performance of MHNFs in engineering applications.

4.2. Onset and completion of transition of different volume fractions of MHNFs and heat transfer enhancement

Theoretical frameworks, such as that proposed by Cengal et al. [38], suggest that the transition regime typically commences at a Critical Reynolds number (Re_{cr})of approximately 2300. However, further investigations by Ghajar and Tam [9], Meyer and Oliver [14] and Nagendra et al. [12], and have revealed that the onset of transition can be influenced by various factors, including fluid properties, geometry of the test section, heat flux, transition length, and inlet configuration. Additionally, Osman et al. [29] observed that the transition begins earlier with single nanofluids compared to base fluids like water, attributed to the heightened fluid viscosity.

To ascertain the beginning of the transitional regime, the critical Re_{cr} for seven MHNFs nanofluids and DIW was determined using a method similar to that described by Everts and Meyer [14], adapted from Cengal et al. [38] and derived from Ghajar and Tam [9] as per Equation (14).

$$\mathrm{Re} = \mathrm{Re}_{cr}, \text{ when } \mathrm{Re} = \left(\frac{dj}{dRe}\right) = 0 \tag{14a}$$

The behavior in the transition region, as described in Table 4, is characterized by two critical Re_{cr} the onset of transition (Re_{cr} onset) and the completion of the transition phase (Re_{cr} completion). Re_{cr} onset denotes the Re at which the flow begins to exhibit signs of shifting from

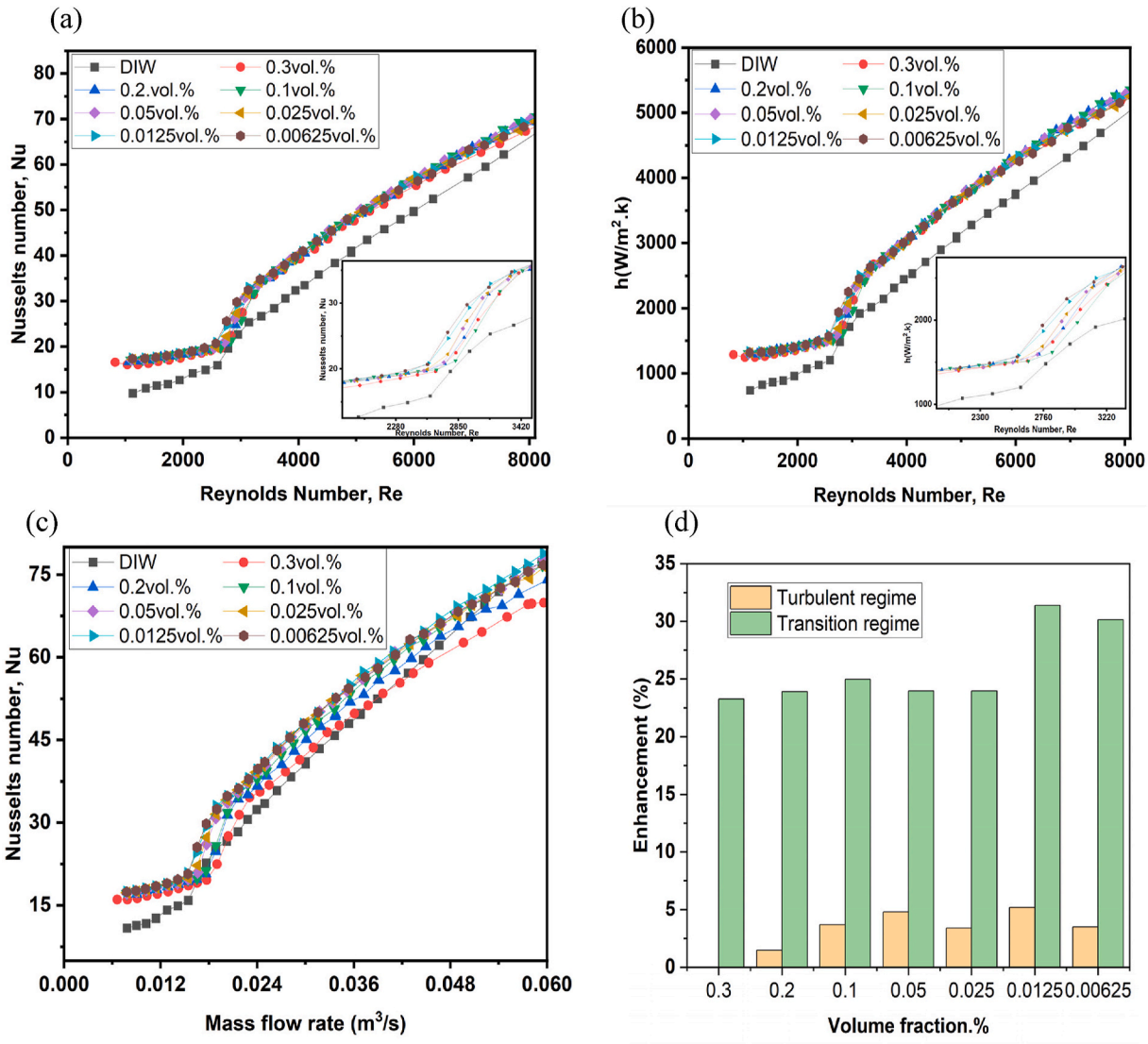

Fig. 8. (A) Comparing Nusselt number results for MHNFS and DIW across Reynolds numbers (b) comparing CHT coefficient outcome of MHNFS to DIW across Reynolds numbers (c) Exploring Nusselt number trends across mass flow rates, DIW and across different MHNFs Nanofluids (d) Comperison of transition and turbulent regime.

Table 4
Impact of volume fraction on the transitional flow regime.

% Volume fraction MHNFs and DIW	Reynold number of the transition flow region	
	onset	completion of the transition phase
0.3	2826.52	3398.47
0.2	2726.65	3323.57
0.1	2822.89	3434.00
0.5	2716.17	3301.61
0.025	2751.74	3318.96
0.0125	2578.26	3141.44
0.00625	2568.67	3126.45
DIW	2592.63	3138.187

laminar to turbulent, marking the lower boundary of the transitional flow regime. On the other hand, Re_{cr} completion signifies the Re, where the flow has fully transitioned to turbulent behaviour, representing the upper boundary of this transitional phase. These critical values vary with the volume fraction of MHNFs and DIW listed in Table 4. Generally, higher volume fractions of MHNFs correspond to higher Re_{cr} values for both the onset and completion of the transition, suggesting that MHNFs can delay the onset of turbulence and alter overall flow dynamics. Notably, even at a volume fraction as low as 0.00625 %, the transition begins at a lower Reynolds number compared to DIW, indicating unique flow characteristics influenced by nanofluid concentration. This variability underscores the significant impact of MHNFs on flow behavior and highlights the importance of understanding these critical Re for fluid system design and operation.

In this study, the transition range for the investigated MHNFs falls within the Re range of 2500–3340, which is within the broader spectrum of 2000–4000, covering both laminar and turbulent flow regimes. Surprisingly, the results indicate that the transition of MHNFs begins at a significantly higher Re compared to DIW, contradicting previous findings by Osman et al. [29], and Mayer et al. [30]. However, in the lowest volume fraction of 0.00625 % Vol, the transition onset started at a lower Re compared to the DIW, which agrees with earlier findings. One possible reason for this disparity could be the specific characteristics of the MHNFs used in this study. Unlike base fluids like DIW, MHNFs are composed of nanoparticles dispersed in a base fluid, altering properties such as viscosity, thermal conductivity, density and volume fraction.

MHNFs begin transitioning at significantly higher Reynolds numbers

compared to previous studies due to several key mechanisms related to their unique thermophysical properties. One of the primary factors is the increased viscosity of MHNFs, particularly those containing magnetic nanoparticles like Fe_3O_4 [26]. The higher viscosity of these fluids increases the resistance to flow, which delays the onset of turbulence. As a result, a higher flow rate and consequently, a higher Reynolds number is needed to overcome the increased viscous forces before the fluid can transition from laminar to turbulent flow. This contrasts with traditional fluids or single-component nanofluids, which typically have lower viscosities and thus transition at lower Reynolds numbers.

Another contributing factor is the behavior of nanoparticle aggregation and the stability of the nanofluids. The hybridization of different nanoparticles can lead to altered aggregation patterns that impact the flow characteristics. In MHNFs, nanoparticles may form clusters that stabilize the laminar flow, delaying the transition to turbulence. This aggregation behavior requires a higher Reynolds number for the flow to become unstable and enter the turbulent regime.

Additionally, the enhanced thermal properties of MHNFs, such as improved thermal conductivity, play a role in delaying the onset of turbulence. The increased thermal conductivity allows the fluid to dissipate heat more effectively in the laminar region, reducing the need for turbulent flow to enhance heat transfer. Consequently, turbulence only becomes necessary at higher Reynolds numbers when the flow reaches more extreme conditions. Finally, the interaction between the nanoparticles and the pipe surface can also influence the transition point. The presence of hybrid nanoparticles can affect the boundary layer thickness near the pipe walls, creating a stabilizing effect that further delays the transition to turbulence. A thicker boundary layer requires a higher flow velocity to become unstable, leading to a higher Reynolds number for the transition.

Overall, the higher Reynolds numbers observed in MHNFs are attributed to the increased viscosity, nanoparticle aggregation, enhanced thermal conductivity, and boundary layer effects, all of which contribute to stabilizing the laminar flow and delaying the onset of turbulence.

Table 4 demonstrates the impact of volume fraction on the transitional flow regime. Different fluid volume fractions exhibit distinct behaviors within this regime. These findings highlight the significant role volume fraction plays in transition. Additionally, nanoparticle dispersion not only enhances the heat transfer properties of the base fluid but also affects other crucial flow characteristics, which are particularly important when designing heat exchangers. Furthermore, the onset and completion of the transition phase also vary with different volume fractions. Fig. 7 (a–c) illustrates the flow regime boundaries for the nanofluids and DIW.

Another factor to consider is the dispersion of nanoparticles within the fluid. Nanoparticles tend to form agglomerates or clusters due to van der Waals forces, which can affect the overall fluid behavior. If the MHNFs in this study had a more homogeneous dispersion of nanoparticles than those studied previously, it could lead to differences in viscosity and other flow properties, consequently affecting the transition behavior. Moreover, the size and shape of nanoparticles can also impact flow dynamics. Since the nanoparticles in the MHNFs investigated in this study were larger and had different shapes compared to those in previous studies, they could affect the fluid's ability to transition from laminar to turbulent flow. Additionally, variations in the concentration of nanoparticles could play a role. Higher nanoparticle concentrations can lead to viscosity and thermal conductivity changes, which may influence the transition to turbulence.

CHT results are illustrated in Fig. 7a and **8**, showcasing the average *Nu* measurements and average CHT coefficients of Fe_3O_4-MgO, MHNFs ranging from 0.3 to 0.00625 vol% compared to DIW across a Re of 1000–8000. CHT coefficient outcomes, as depicted in Figs. 7(a) and **8**, indicate an improvement in heat transfer within the fully developed turbulent regime. Notably, at a Re of 8000, no enhancement was noticed for the 0.3 vol% MHNFs, while enhancements of 1.46 %, 3.69 %, 4.79 %, 3.4 %, 5.2 %, and 3.48 % were observed for MHNF concentrations of 0.2 vol%, 0.1 vol%, 0.05 vol%, 0.025 vol%, 0.0125 vol%, and 0.00625 vol %, respectively.

The average enhancements in Nusselt numbers were 0 % for 0.3 vol% and 0.2 vol%, 2.97 % for 0.1 vol%, 3.9 % for 0.05 vol%, 3.2 % for 0.025 vol%, 5.1 % for 0.0125 vol%, and 3.4 % for 0.00625 vol% MHNFs.

The transition into enhanced heat transfer began at Reynolds numbers of 2643, 2726, 2649, 2716, 2751, 2578, and 2568 for MHNF concentrations of 0.3 vol%, 0.2 vol%, 0.1 vol%, 0.05 vol%, 0.025 vol%, 0.0125 vol%, and 0.00625 vol%, respectively. In the transition flow regime, enhancements in Nusselt number were found to be 23.27 %, 23.90 %, 24.97 %, 23.96 %, 23.96 %, 31.38 %, and 30.13 % for the respective MHNF concentrations.

Comparing enhancements in heat transfer between the turbulent and transition flow regimes showed that heat exchange was more pronounced in the transition region as shown in Fig. 7(d). The average enhancements in heat transfer were 26 % for 0.3 vol%, 25.8 % for 0.2 vol %, 25.7 % for 0.1 vol%, 17.9 % for 0.05 vol%, 25.6 % for 0.025 vol%, 31.6 % for 0.0125 vol%, and 30.2 % for 0.00625 vol% MHNFs. Interestingly, the optimum enhancement was observed with MHNF concentrations of 0.0125 vol% and 0.00625 vol%.

One potential rationale for the heightened improvement in the transition flow domain, particularly evident at increased volume fractions, could be attributed to the role of Brownian motion in nanoparticles and the stochastic nature of flow, aiding in their integration with the base fluid. Additionally, the incorporation of smaller particles into the base fluid might suppress turbulence by acting as an extra source of dissipation, in line with the suggestion made by Hetsroni [44].

The improvement observed in the laminar domain was notably significant, with average enhancements in heat transfer ranging from 11 % for 0.3 vol% MHNFs to 80.0 % for 0.0125 vol% MHNFs, and 78 % for 0.00625 vol% MHNFs. This trend is in line with previous research that also reported enhancement in laminar flow for fully developed conditions.

One possible reason for the higher enhancement in the laminar region juxtaposed to the transition and turbulent domain for MHNFs could be attributed to the behaviour of nanoparticles in laminar flow conditions. In laminar flow, the motion of fluid particles is more orderly and predictable, allowing nanoparticles to interact with the fluid and promote heat transfer effectively. Additionally, the absence of turbulent fluctuations may enable nanoparticles to exert a more consistent influence on heat transfer, leading to higher enhancements. Furthermore, the unique characteristics of MHNFs, such as particle size, shape, and dispersion, may exhibit a more prominent impact on heat exchange in laminar flow conditions, contributing to the observed higher enhancements.

4.3. Analysis of pressure drop (Δp) behavior of MHNFS, friction factor variation with Reynolds number and particle volume fraction across flow regimes

Fig. 9 a, illustrates the Δp of Fe_3O_4-MgO MHNFs range from 0.3 to 0.00625 vol% compared to DIW against the flow rate across the entire flow range; in the turbulent regime, fluid flow is characterized by chaotic and irregular motion, leading to higher frictional forces and, thus, higher pressure drops. For various volume fractions in this regime, the maximum pressure drops are depleted in Table 5. This table provides the maximum pressure drops for each flow regime, considering different volume fractions and flow rates. This gives a comprehensive view of how the Δp varies with changing flow conditions and volume fractions.

The pressure drop (Δp) tends to rise with increasing nanoparticle volume fraction, reaching its maximum at 0.025 % volume at a flow rate of 0.05257, before slightly declining at higher concentrations. This peak likely reflects increased turbulence and particle-fluid interactions, which amplify frictional forces. These results are consistent with Prakash et al. [45], who observed that the friction factor of nanofluids

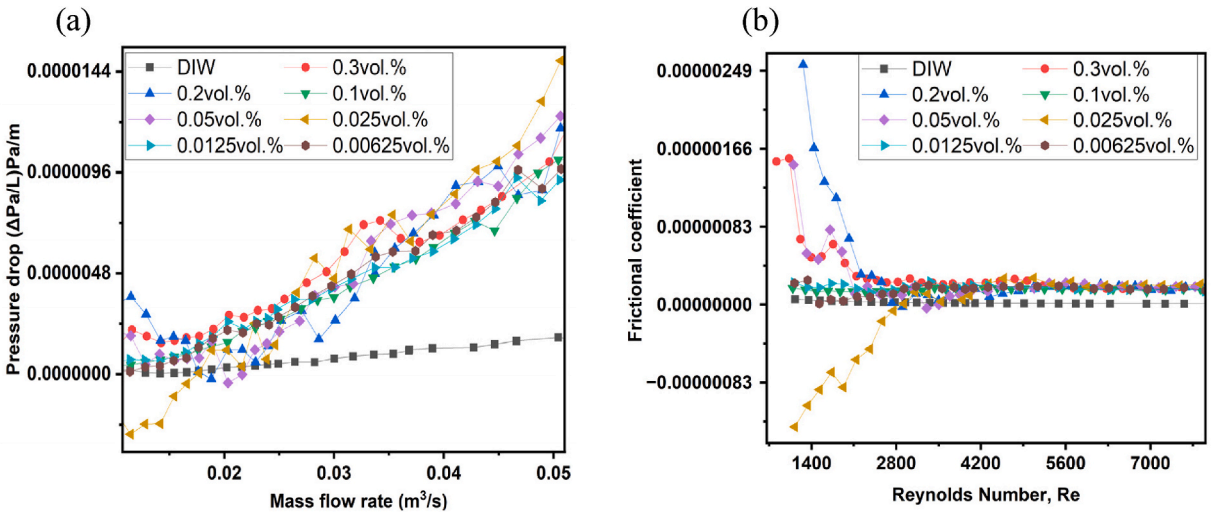

Fig. 9. (A) Pressure drop of Fe_3O_4-MgO MHNFs compared to DIW across flow regimes (b) friction factor variation with Reynolds number and particle volume fraction across flow regimes.

Table 5
Maximum pressure drops across flow regimes with different volume fractions and flow rates.

% Volume fraction	Maximum Δ*p* Laminar flow	Flow rate (l/m) Laminar regime	Maximum Δ*p* Transition flow	Flow rate (l/m) Transition regime	Maximum Δ*p* Turbulet flow	Flow rate (l/m) Turbulet regime
0.3	1.5×10^{-6}	0.01423	2.82×10^{-6}	0.020412	1.1×10^{-5}	0.055034
0.2	1.6×10^{-6}	0.01646	5.81×10^{-7}	0.022836	1.34×10^{-5}	0.052427
0.1	8.31×10^{-7}	0.01541	$2.04. \times 10^{-6}$	0.021641	1.02×10^{-5}	0.052219
0.05	6.43×10^{-7}	0.01544	-1.3×10^{-8}	0.021619	1.27×10^{-5}	0.05241
0.025	-1.1×10^{-6}	0.01543	3.72×10^{-7}	0.021602	1.48×10^{-5}	0.05257
0.0125	8.31×10^{-7}	0.01569	2.14×10^{-6}	0.021738	1.06×10^{-5}	0.052427
0.00625	6.52×10^{-7}	0.01539	1.98×10^{-6}	0.021679	1.09×10^{-5}	0.052359

increases with higher nanoparticle concentrations but decreases as the Reynolds number and inlet fluid temperature rise.

In the transitional regime, the flow behavior fluctuates between laminar and turbulent characteristics, resulting in varying frictional forces and pressure drops. The maximum pressure drops for various volume fractions as deplected in Table 5 were 0.3 % Vol at a flow rate of 0.020412. The pressure drops in the transitional regime are generally lower and more consistent across different volume fractions compared to the turbulent regime, indicating less pronounced effects of particle concentration on Δp in transitional flow.

In the laminar regime, fluid flow is smooth and orderly except for 0.025 % vol, with minimal mixing and lower frictional forces, leading to lower Δp. The maximum pressure drops for various volume fractions were: 0.2 % Vol, as shown in Table 5, at a flow rate of 0.01646. In the laminar regime, the Δp are significantly lower than the other regimes and show minimal variation with changes in volume fraction, as the flow is stable and the particles have a minor impact on the frictional forces.

Flow structure also plays a crucial role, turbulent flow enhances mixing and particle-fluid interactions, amplifying pressure drops. Transitional flow structures exhibit less chaotic behavior, resulting in more stable but less intense interactions. Laminar flow structures are stable and orderly, with minimal mixing and interaction, resulting in the lowest pressure drops. Reynolds number effects further explain these variations: higher Reynolds numbers (indicating turbulent flow) generally correlate with higher pressure drops due to increased momentum exchange and friction. In transitional regimes, lower Reynolds numbers lead to flow alternating between laminar and turbulent states, resulting in lower and more stable pressure drops. Low Reynolds numbers indicate smooth flow in laminar regimes, contributing to the lowest pressure drops.

Particle settling and distribution also contribute: turbulent regimes produce more uniform particle distribution due to intense mixing, resulting in higher resistance and pressure drops. Transitional regimes may see more particle settling or clustering due to reduced mixing, contributing to lower overall pressure drops. Laminar regimes show minimal particle movement and settling due to the lack of mixing, minimally affecting pressure drops.

In summary, pressure drop behavior varies significantly across turbulent, transitional, and laminar regimes due to differences in flow characteristics and particle interactions. Turbulent regimes exhibit higher and more variable pressure drops due to chaotic flow and intensified particle interactions, often peaking at specific volume fractions. Transitional regimes show lower and more consistent pressure drops, reflecting less intense and more stable flow conditions. Laminar regimes display the lowest and most stable pressure drops due to smooth, orderly flow with minimal particle interactions.

Fig. 9(b), illustrates significant variations in the friction factor based on different volume fractions. The Reynolds number remains relatively constant at higher volume fractions (0.3 %–0.00625 % Vol), yet the friction factor varies noticeably. For instance, at a 0.3 % volume fraction, the friction factor ranges from 1.54×10^{-7} to 1.52×10^{-6} across various Reynolds numbers. This indicates that with higher concentrations of particles or structures in the fluid, the friction factor tends to increase due to more pronounced particle interaction and obstruction, leading to greater flow resistance. As the volume fraction decreases from 0.3 % to 0.025 % Vol, the friction factors decrease slightly, approaching the behavior of a pure fluid, with values such as 1.53×10^{-7} at a 0.2 % volume fraction and 1.41×10^{-7} at a 0.1 % volume fraction. Even at these lower concentrations, the friction factor still shows observable variability, suggesting that small concentrations of particles can still influence fluid dynamics. The differences in friction factors are more pronounced in the transition and turbulent regimes than in the laminar

regime. In the transition regime, where the flow is unstable and moving towards turbulence, and in the fully developed turbulent regime, where chaotic fluid movements and interactions are dominant, particles significantly affect the friction factor. In contrast, in the laminar regime, where the flow is smooth and orderly, the impact of volume fraction on the friction factor is less significant. Thus, volume fraction changes in the transition and turbulent flow regimes most significantly affect the friction factor.

Furthermore, the assessment of The Total Efficiency Index (TEI) can serve as a valuable metric for evaluating the performance of Fe_3O_4/MgO nanofluids in heat transfer systems. The TEI is defined as follows [46].

$$\eta = \frac{\frac{h_{avg,bf}}{h_{avg,nf}}}{\frac{\Delta P_{nf}}{\Delta P_{bf}}} \quad 12$$

Fig. 10 illustrates the thermal efficiency across flow regimes for MHNFs at various volume fractions, revealing intriguing trends. Interestingly, The Total Efficiency Index (TEI) for Fe_3O_4-MgO nanofluids at various volume fractions and flow regimes provides a detailed perspective on their heat transfer performance. At a volume fraction of 0.00625 %, TEI values are slightly above 1.00 across Reynolds numbers, indicating decent thermal efficiency. Specifically, the TEI values are 1.02 in turbulent flow, 1.23 in transition flow, and 1.26 in laminar flow. These results suggest that the nanofluid enhances heat transfer effectively even at low concentrations.

Increasing the volume fraction to 0.0125 % results in a notable rise in TEI values, indicating improved efficiency. At this concentration, TEI values reach 1.04 in turbulent flow, 1.25 in transition flow, and 1.264 in laminar flow. This concentration provides the highest efficiency across all regimes, demonstrating that a slight increase in concentration significantly enhances nanofluid performance.

At a volume fraction of 0.025 %, TEI values remain high across different flow regimes, with values of 1.01 in turbulent flow, 1.23 in transition flow, and 1.24 in laminar flow. This concentration continues to improve thermal performance, although there is a slight decrease in turbulent flow efficiency compared to 0.0125 %, which could be attributed to increased viscosity or particle interactions at higher concentrations.

Further increasing the concentration to 0.05 % results in TEI values of 1.017 in turbulent flow, 1.21 in transition flow, and 1.22 in laminar flow. While these values indicate enhanced efficiency, the slightly lower performance in turbulent flow compared to 0.025 % suggests that very high concentrations might introduce drawbacks such as increased viscosity or particle aggregation.

At a volume fraction of 0.1 %, the TEI values are 0.997 in turbulent flow, 1.17 in transition flow, and 1.21 in laminar flow. This concentration exhibits the highest TEI values in the transition regime, suggesting it is near optimal for maximizing heat transfer efficiency. However, the observed decrease in efficiency during turbulent flow at this concentration implies that higher nanoparticle concentrations may increase fluid resistance or introduce other adverse effects. These findings align with those of Kumar et al. [47], where nanofluids enhanced TEI in the turbulent regime but experienced a decline in performance with increasing Reynolds numbers and particle concentrations. At a higher volume fraction of 0.2 %, TEI values drop to 0.940 in turbulent flow, 1.08 in transition flow and 1.07 in laminar flow. This decrease in efficiency, particularly in turbulent and transition flows, could be due to excessively high viscosity, poor particle dispersion, or other factors that hinder the nanofluid's performance. Despite a slight increase in laminar flow efficiency, the overall performance is reduced compared to lower concentrations.

Finally, TEI values are the lowest at the highest tested volume fraction of 0.3 %, with 0.857 in turbulent flow, 0.934 in transition flow, and 1.17 in laminar flow. This indicates that the nanofluid becomes less effective at very high concentrations due to increased viscosity, sedimentation, or other adverse effects on fluid dynamics.

In summary, a % volume fraction of 0.0125 vol% provides the best overall performance across various flow regimes, particularly in the transition flow regime. As the volume fraction increases beyond this optimal point, efficiency generally decreases due to increased viscosity and other factors affecting fluid dynamics.

5. Conclusion

This study examined the heat transfer characteristics of Fe_3O_4-MgO/DIW Magnetic Hybrid Nanofluids (MHNFs) compared to deionized water (DIW) across various flow regimes. Key findings include the following:

- The transition range for MHNFs occurs at significantly higher Reynolds numbers compared to DIW and single nanofluids, suggesting that MHNFs' unique thermophysical properties influence flow behavior.
- Colburn j factors were more affected by viscosity, likely due to its influence on the Prandtl number. Nanofluids with the highest stability and heat transfer efficiency exhibited the highest Colburn j factors.
- The transition flow regime exhibited the most significant enhancements in heat transfer efficiency, with an optimal volume fraction of

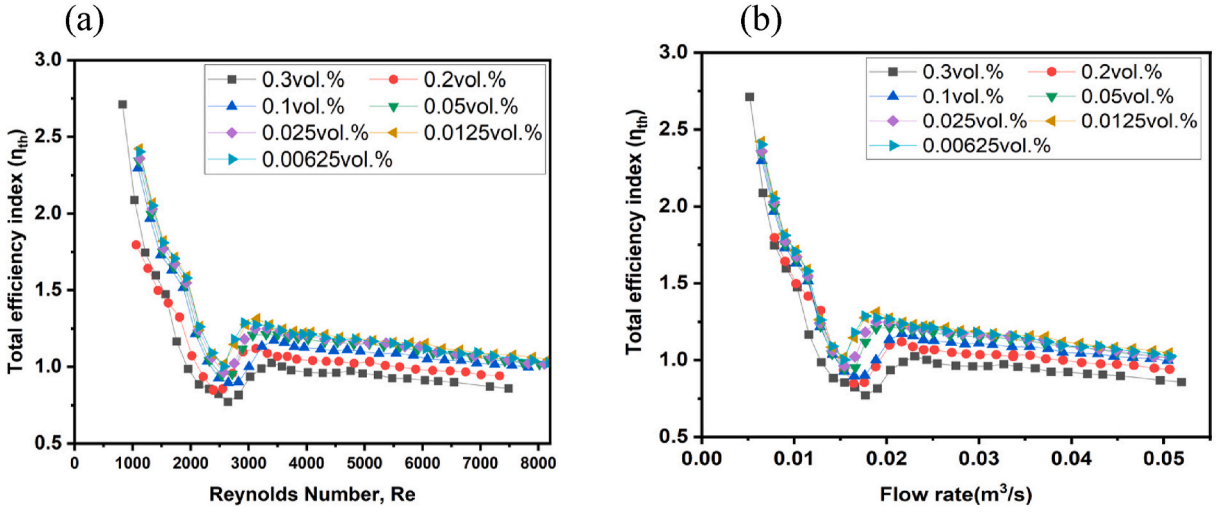

Fig. 10. Influence of flow regime and volume fraction on thermal efficiency of Fe_3O_4-MgO MHNF.

approximately 0.0125 vol%. Convection heat transfer efficiency improvements ranged from 23.27 % for 0.3 vol% MHNFs to 31.38 % for 0.0125 vol%.
- The Total Efficiency Index (TEI) revealed that the highest thermal efficiency was achieved at a concentration of 0.0125 % across all flow regimes. Increasing the volume fraction beyond this point led to a reduction in TEI, particularly in turbulent flows, likely due to increased viscosity and potential particle aggregation.

The results underscore the importance of optimizing nanofluid concentration for practical applications. The TEI values indicate that a volume fraction of 0.0125 % strikes the best balance between enhancing heat transfer efficiency and maintaining stable fluid dynamics. For real-world applications in cooling systems, heat exchangers, or energy systems, this concentration can provide maximum thermal efficiency while minimizing negative effects such as increased pressure drops or higher pumping energy requirements. The findings provide valuable insights for industries aiming to improve thermal performance using MHNFs.

- Enhanced efficiency in heat transfer systems, The significant improvements in heat transfer efficiency, particularly in the transition flow regime, suggest that MHNFs could be highly effective in applications where efficient thermal management is critical, such as in heat exchangers, cooling systems, and industrial processes. The findings emphasize the importance of optimizing the volume fraction (e.g., 0.0125 vol%) to achieve the best performance.
- practical applications in engineering, The study shows that higher Reynolds numbers are required to initiate the transition in MHNFs compared to conventional fluids, which implies that MHNFs could be more suitable for systems operating at high Reynolds numbers, where conventional fluids may fall short in performance. This highlights the potential for using MHNFs in advanced engineering systems, particularly those requiring high thermal efficiency.
- Viscosity and stability management, Given that viscosity significantly impacts the Colburn j factor, careful management of nanoparticle concentration and fluid viscosity is recommended to optimize heat transfer performance. While higher concentrations increase viscosity and may reduce performance, lower concentrations, such as 0.0125 vol%, appear optimal.
- Design of dvanced nanofluid systems, The study's results suggest that future work should focus on refining nanofluid formulations to balance viscosity, stability, and thermal conductivity. This will ensure maximum heat transfer efficiency while minimizing pressure drops and maintaining stability over time.
- Further research, Continued research into the interaction between nanoparticles and fluid properties, particularly in terms of particle shape, size, and surface modification, will be crucial for enhancing MHNF performance. Additionally, exploring the long-term stability of MHNFs in various operational conditions will be necessary to ensure their viability in real-world applications.

These recommendations emphasize the practical benefits of MHNFs in improving heat transfer systems and provide direction for future research and application in the field.

Al	Aluminium nanoparticles
AL_2O_3	Aluminium oxide nanoparticles
Au	Gold nanoparticles
C_p	Specific heat transfer
Co_2O_3	Cobalt (III) oxide nanoparticles
Cu	Copper nanoparticles
CuO	Copper oxide nanoparticles
CHT	Convective heat transfer
CNTs	Carbon nanotubes
DC	Direct current
Di	Internal diameter of the tube
DIW	Deionized water
DW	Distilled water
EG	Ethylene glycol
Fe_2O_3	Iron (III) oxide nanoparticles
Fe_3O_4	Iron (IV) oxide nanoparticles
G	Gauss
GA	Gum Arabic
GMO	Graphene magnetite oxide
I	Current (Ampere)
$\dot{m}$	Mass flow rate
MF	Magnetic fields
MHNFs	Magnetic hybrid nanofluids
MNFs	Magnetic nanofluids
MNPs	Magnetic nanoparticles
MWCNT	Multiwalled carbon nanoparticle
$\dot{q}$	Heat flux, W /m^2
SF	Sedimentation Factor
SiO_2	Silicon oxide nanoparticles
TEM	Transmission electron microscopy
Ti O_2	Titanium oxide nanoparticles
TEI	Total efficiency index
UV–Vis	Ultra Violet-Visible
V	Voltage
x/d	Axial distance

Greek symbols

φ	Mass ratio of nanofluids
Φ	Volume concentration (vol%)
μ	Viscosity (kg/m.s)
κ	Thermal conductivity (Wm/K-1)
σ	Electrical conductivity (mS/cm −1)
ρ	Density (Kg /m^3)
η	Thermal efficiency
$\dot{q}$	Heat flux, (W /m^2)
$\dot{m}$	Mass flow rate (Kg/s)

Subscripts

A_o	Initial Absorbance
A_t	Final Absorbance
avg	Average
u_B	Bias error
u_p	Precision error
bf	base fluid
C_p	Specific heat capacity of particles (J/kg-K)
C_{pnf}	specific heat capacity of nanofluids (J/kg-K)
C_{pbf}	specific heat capacity of base fluids (J/kg-K)
C_{pnp}	specific heat capacity of nanoparticles (J/kg-K)
ρ_{nf}	Densities of the nanofluid (Kg /m^3)
ρ_{bf}	Density of base fluid (Kg /m^3)
$\varphi\rho_{np}$	Density of nanoparticles (Kg /m^3)
h_{avg}	Average heat transfer coefficient (W /m^2-K)
T_O	outlet °C
T_i	inlet °C
t_w	wall temperature °C
t_b	bulk temperature °C
n_f	nanofluid
n_p	nanoparticles

Dimensionless Numbers

Nu	Nusselt number
Re	Reynold number
Pr	Prandtl number

CRediT authorship contribution statement

Victor O. Adogbeji: Writing – original draft, Validation, Investigation, Formal analysis, Data curation, Conceptualization. **Mohsen Sharifpur:** Writing – review & editing, Validation, Supervision, Resources, Project administration, Methodology, Funding acquisition, Formal analysis. **Josua P. Meyer:** Writing – review & editing, Supervision, Methodology, Formal analysis.

Declaration of competing interest

The authors affirm that they do not have any known monetary interests or personal relationships that might be perceived as influencing the work presented in this paper.

Data availability

Data will be made available on request.

References

[1] S.U.S. Choi, J.A. Eastman, Enhancing thermal conductivity of fluids with, ASME Int Mech Eng Congr Expo 66 (1995) 99–105, https://doi.org/10.1115/1.1532008.

[2] M. Ahmed, M. Eslamian, Laminar forced convection of a nanofluid in a microchannel: effect of flow inertia and external forces on heat transfer and fluid flow characteristics, Appl. Therm. Eng. 78 (Mar. 2015) 326–338, https://doi.org/10.1016/J.APPLTHERMALENG.2014.12.069.

[3] C.H. Peng, Y.X. Liu, L.Z. Zhang, Radiation-convective heat transfer and performance analysis of a parallel-plates duct direct absorption solar heat collection system, Appl. Therm. Eng. 245 (May 2024) 122796, https://doi.org/10.1016/J.APPLTHERMALENG.2024.122796.

[4] S. Nasir, A. Berrouk, Z. Khan, Efficiency assessment of thermal radiation utilizing flow of advanced nanocomposites on riga plate, Appl. Therm. Eng. 242 (Apr. 2024) 122531, https://doi.org/10.1016/J.APPLTHERMALENG.2024.122531.

[5] L. Shi, Y. Hu, Y. He, Magnetocontrollable convective heat transfer of nanofluid through a straight tube, Appl. Therm. Eng. 162 (March) (2019) 114220, https://doi.org/10.1016/j.applthermaleng.2019.114220.

[6] Z. Narankhishig, J. Ham, H. Lee, H. Cho, Convective heat transfer characteristics of nanofluids including the magnetic effect on heat transfer enhancement - a review, Appl. Therm. Eng. 193 (April) (2021) 116987, https://doi.org/10.1016/j.applthermaleng.2021.116987.

[7] A.J. Ghajar, K.F. Madon, Pressure drop measurements in the transition region for a circular tube with three different inlet configurations, Exp. Therm. Fluid Sci. 5 (1) (1992) 129–135, https://doi.org/10.1016/0894-1777(92)90062-A.

[8] A.J. Ghajar, L.-M. Tam, Flow Regime Map for a Horizontal Pipe with Uniform Wall Heat Flux and Three Inlet Configurations, Exp. Therm. Fluid Sci. 10 (1995) 287–297. Elsevier Science Inc., 655 Avenue of the Americas, New York, NY 10010.

[9] A.J. Ghajar, L.M. Tam, Heat transfer measurements and correlations in the transition region for a circular tube with three different inlet configurations, Exp. Therm. Fluid Sci. 8 (1) (1994) 79–90, https://doi.org/10.1016/0894-1777(94)90075-2.

[10] L-M. Tam, A.J. Ghajar, Effect of Inlet Geometry and Heating on the Fully Developed Friction Factor in the Transition Region of a Horizontal Tube, Exp. Therm. Fluid Sci. 15 (1997) 52–64. Elsevier Science Inc., 0894-1777/97/$17.00 655 Avenue of the Americas, New York, NY 10010.

[11] H.K. Tam, L.M. Tam, A.J. Ghajar, Effect of inlet geometries and heating on the entrance and fully-developed friction factors in the laminar and transition regions of a horizontal tube, Exp. Therm. Fluid Sci. 44 (2013) 680–696, https://doi.org/10.1016/j.expthermflusci.2012.09.008.

[12] H.R. Nagendra, Interaction of free and forced convection in horizontal tubes in the transition regime, J. Fluid Mech. 57 (2) (1973) 269–288, https://doi.org/10.1017/S0022112073001151.

[13] J.P. Meyer, J.A. Olivier, Transitional flow inside enhanced tubes for fully developed and developing flow with different types of inlet disturbances: Part II-heat transfer, Int. J. Heat Mass Tran. 54 (7–8) (2011) 1598–1607, https://doi.org/10.1016/j.ijheatmasstransfer.2010.11.026.

[14] J.P. Meyer, J.A. Olivier, Transitional flow inside enhanced tubes for fully developed and developing flow with different types of inlet disturbances: Part I - adiabatic pressure drops, Int. J. Heat Mass Tran. 54 (7–8) (2011) 1587–1597, https://doi.org/10.1016/j.ijheatmasstransfer.2010.11.027.

[15] M. Everts, J.P. Meyer, Heat transfer of developing flow in the transitional flow regime, Proc. Therm. Fluids Eng. Summer Conf. 2015-Augus (d) (2015) 1051–1063, https://doi.org/10.1615/tfesc1.fnd.012660.

[16] J.P. Meyer, M. Everts, Single-phase mixed convection of developing and fully developed flow in smooth horizontal circular tubes in the laminar and transitional flow regimes, Int. J. Heat Mass Tran. 117 (Feb. 2018) 1251–1273, https://doi.org/10.1016/j.ijheatmasstransfer.2017.10.070.

[17] M. Everts, J.P. Meyer, Flow regime maps for smooth horizontal tubes at a constant heat flux, Int. J. Heat Mass Tran. 117 (2018) 1274–1290, https://doi.org/10.1016/j.ijheatmasstransfer.2017.10.073.

[18] S. Osman, M. Sharifpur, and J. P. Meyer, "The effect of chopping the boundary layer at the inlet on the transition heat transfer and pressure drop characteristics in smooth horizontal tube." [Online]. Available: https://www.researchgate.net/publication/335611932.

[19] A. Lee, C. Veerakumar, H. Cho, Effect of magnetic field on the forced convective heat transfer of water–ethylene glycol-based fe3 o4 and fe3 o4 –mwcnt nanofluids, Appl. Sci. 11 (10) (May 2021), https://doi.org/10.3390/app11104683.

[20] F. Selimefendigil, H.F. Öztop, N. Abu-Hamdeh, Optimization of phase change process in a sinusoidal-wavy conductive walled cylinder with encapsulated-phase change material during magnetohydrodynamic nanofluid convection, J. Energy Storage 55 (PC) (2022) 105512, https://doi.org/10.1016/j.est.2022.105512.

[21] H. Talebi, V. Kalantar, Nazari, M.R. Kargarsharifabad, Experimental investigation of the forced convective heat transfer of hybrid Cu/Fe3O4 nanofluids, J. solid Fluid Mech. 8 (4) (2019) 229–238, https://doi.org/10.22044/jsfm.2019.7350.2687.

[22] L.S. Sundar, H.M. Abebaw, M.K. Singh, A.M.B. Pereira, A.C.M. Sousa, Experimental heat transfer and friction factor of Fe3O4 magnetic nanofluids flow in a tube under laminar flow at high Prandtl numbers, Int. J. Heat Technol. 38 (2) (2020) 301–313, https://doi.org/10.18280/ijht.380204.

[23] A. Shahsavar, M. Saghafian, M.R. Salimpour, M.B. Shafii, Experimental investigation on laminar forced convective heat transfer of ferrofluid loaded with carbon nanotubes under constant and alternating magnetic fields, Exp. Therm. Fluid Sci. 76 (Sep. 2016) 1–11, https://doi.org/10.1016/j.expthermflusci.2016.03.010.

[24] F. Selimefendigil, H.F. Öztop, Hybrid nanofluid convection and phase change process in an expanded channel under the combined effects of double rotating cylinders and magnetic field, J. Mol. Liq. 368 (2022) 120364, https://doi.org/10.1016/j.molliq.2022.120364.

[25] S. Askari, H. Koolivand, M. Pourkhalil, R. Lotfi, A. Rashidi, Investigation of Fe3O4/Graphene nanohybrid heat transfer properties: experimental approach, Int. Commun. Heat Mass Tran. 87 (July) (2017) 30–39, https://doi.org/10.1016/j.icheatmasstransfer.2017.06.012.

[26] L.S. Sundar, M.K. Singh, A.C.M. Sousa, Enhanced heat transfer and friction factor of MWCNT-Fe3O4/water hybrid nanofluids, Int. Commun. Heat Mass Tran. 52 (Mar. 2014) 73–83, https://doi.org/10.1016/j.icheatmasstransfer.2014.01.012.

[27] M.H. Aghabozorg, A. Rashidi, S. Mohammadi, Experimental investigation of heat transfer enhancement of Fe2O3-CNT/water magnetic nanofluids under laminar, transient and turbulent flow inside a horizontal shell and tube heat exchanger, Exp. Therm. Fluid Sci. 72 (Apr. 2016) 182–189, https://doi.org/10.1016/j.expthermflusci.2015.11.011.

[28] S.S. Chougule, V. V Nirgude, P.D. Gharge, M. Mayank, S.K. Sahu, Heat transfer enhancements of low volume concentration CNT/water nanofluid and wire coil inserts in a circular tube, Energy Proc. 90 (2016) 552–558, https://doi.org/10.1016/j.egypro.2016.11.223.

[29] S. Osman, M. Sharifpur, J.P. Meyer, Experimental investigation of convection heat transfer in the transition flow regime of aluminium oxide-water nanofluids in a rectangular channel, Int. J. Heat Mass Tran. 133 (2019) 895–902, https://doi.org/10.1016/j.ijheatmasstransfer.2018.12.169.

[30] J.P. Meyer, T.J. McKrell, K. Grote, The influence of multi-walled carbon nanotubes on single-phase heat transfer and pressure drop characteristics in the transitional flow regime of smooth tubes, Int. J. Heat Mass Tran. 58 (1–2) (2013) 597–609, https://doi.org/10.1016/j.ijheatmasstransfer.2012.11.074.

[31] I.U. Ibrahim, M. Sharifpur, J.P. Meyer, S.M.S. Murshed, Experimental investigations of effects of nanoparticle size on force convective heat transfer characteristics of Al2O3 - MWCNT hybrid nanofluids in transitional flow regime, Int. J. Heat Mass Tran. 228 (June 2023) (2024) 125597, https://doi.org/10.1016/j.ijheatmasstransfer.2024.125597.

[32] S.O. Giwa, M. Sharifpur, M.H. Ahmadi, S.M. Sohel Murshed, J.P. Meyer, Experimental investigation on stability, viscosity, and electrical conductivity of water-based hybrid nanofluid of mwcnt-fe2o3, Nanomaterials 11 (1) (Jan. 2021) 1–19, https://doi.org/10.3390/nano11010136.

[33] A. Arifutzzaman, A.F. Ismail, I.I. Yaacob, M.Z. Alam, A.A. Khan, Stability investigation of water based exfoliated graphene nanofluids, IOP Conf. Ser. Mater. Sci. Eng. 488 (1) (2019), https://doi.org/10.1088/1757-899X/488/1/012002.

[34] S.S.J. Aravind, P. Baskar, T.T. Baby, R.K. Sabareesh, S. Das, S. Ramaprabhu, Investigation of structural stability, dispersion, viscosity, and conductive heat transfer properties of functionalized carbon nanotube based nanofluids, J. Phys. Chem. C 115 (34) (2011) 16737–16744, https://doi.org/10.1021/jp201672p.

[35] S. Chakraborty, P.K. Panigrahi, Stability of nanofluid: a review, Appl. Therm. Eng. 174 (2020), https://doi.org/10.1016/j.applthermaleng.2020.115259.

[36] E.O. Atofarati, M. Sharifpur, J. Meyer, Hydrodynamic effects of hybrid nanofluid jet on the heat transfer augmentation, Case Stud. Therm. Eng. 51 (July) (2023) 103536, https://doi.org/10.1016/j.csite.2023.103536.

[37] J.V. Sengers, J.T.R. Watson, Improved international formulations for the viscosity and thermal conductivity of water substance, J. Phys. Chem. Ref. Data 15 (4) (Oct. 1986) 1291–1314, https://doi.org/10.1063/1.555763.

[38] J. Çengel, A. Yunus, Afshin Ghajar, Heat and Mass Transfer in SI Units: Fundamentals and Applications, sixth ed., MCGraw Hill, 2020.

[39] B.C. Pak, Y.I. Cho, Hydrodynamic and heat transfer study of dispersed fluids with submicron metallic oxide particles, Exp. Heat Tran. 11 (2) (1998) 151–170, https://doi.org/10.1080/08916159808946559.

[40] F.W. Dittus, L.M.K. Boelter, Heat transfer in automobile radiators of the tubular type, Int. Commun. Heat Mass Tran. 12 (1) (1985) 3–22, https://doi.org/10.1016/0735-1933(85)90003-X.

[41] E.N. Sieder, G.E. Tate, Heat transfer and pressure drop of liquids in tubes, Ind. Eng. Chem. 28 (12) (1936) 1429–1435, https://doi.org/10.1021/ie50324a027.

[42] V. Gnielinski, New equation for heat and mass transfer in turbulent and channel flow, Ind. Eng. Chem. Res. 16 (12) (1976) 359–368. https://cir.nii.ac.jp/crid/1571980075607043456.bib?lang=en.
[43] P.F. Dunn, Measurement and Data Analysis for Engineering and Science, Second Edition, Taylor and Francis/CRC Press, 2010, pp. 1–7, c2010, ISBN: 9781439825686, no. August 2009.
[44] G. Hetsroni, Particles-turbulence interaction, Int. J. Multiphas. Flow 15 (5) (1989) 735–746, https://doi.org/10.1016/0301-9322(89)90037-2.
[45] M. H B, P.K. Kanti, S.B. Prakash, S.N. Sridhara, Investigation of entropy generation and thermohydraulic characteristics of Al2O3–CuO hybrid nanofluid flow in a pipe at different inlet fluid temperatures, Int. J. Therm. Sci. 193 (July) (2023) 108541, https://doi.org/10.1016/j.ijthermalsci.2023.108541.
[46] M. Goharkhah, M. Ashjaee, M. Shahabadi, Experimental investigation on convective heat transfer and hydrodynamic characteristics of magnetite nanofluid under the influence of an alternating magnetic field, Int. J. Therm. Sci. 99 (2016) 113–124, https://doi.org/10.1016/j.ijthermalsci.2015.08.008.
[47] P. Kumar K, M. Alruqi, H.A. Hanafi, P. Sharma, V.V. Wanatasanappan, Effect of particle size on second law of thermodynamics analysis of Al2O3 nanofluid: application of XGBoost and gradient boosting regression for prognostic analysis, Int. J. Therm. Sci. 197 (July 2023) (2024) 108825, https://doi.org/10.1016/j.ijthermalsci.2023.108825.